EVALUATION OF THE RADIATION DETECTION PROPERTIES OF SYNTHETIC DIAMONDS FOR MEDICAL APPLICATIONS

Nicholas Ade

A thesis submitted to the Faculty of Science, University of the Witwatersrand, Johannesburg, in fulfilment of the requirements for the degree of Doctor of Philosophy.

Johannesburg, 2015

DECLARATION

I declare that this thesis is my own, unaided work. It is being submitted for the Degree of Doctor of Philosophy in the University of the Witwatersrand, Johannesburg. It has not been submitted before for any degree or examination in any other University.

_____

30th day of January 2015

ABSTRACT

Aimed at improving the accuracy of dose determination in radiation medicine, this thesis explores the radiation detection properties of synthetic diamond crystals of various types and investigates the possibility of developing a single probe with synthetic diamond as sensor for the dosimetry of various beam types under large as well as small-field conditions. The study was conducted on two HPHT (high-pressure, high-temperature) and eight CVD (chemical vapour deposited) synthesised diamonds of optical grade (OG) and detector grade (DG) qualities of various dimensions. Various non-destructive techniques were employed to characterise the electrical quality and some defect levels present within each of the samples.

Detector performances were evaluated using a prototype probe housing constructed of tissue-equivalent materials. The probe has features which allow diamond crystals to be exposed in different exposure orientations ('edge-on' and 'flat-on') for impinging radiation without having first to re-orient the diamond sensor within its body. All dosimetric measurements taken with the synthetic diamond probe were from exposures to low-energy mammography X-rays (25-32 kVp), and megavoltage therapy electron (7-14 MeV) and photon (^{60}Co γ-ray, 6 and 15 MV X-ray) beams.

The most important findings emphasized in this thesis include:

(1) The main cause of the instability of response of the examined crystals necessitating the often cited daily primimg procedure was isolated and ascribed to the presence of ambient light which has the effect of emptying trapping centres present within the diamond sensors. The percentage changes in response between measurements in light and dark conditions conducted over a period of three successive weeks were 2.8±1.2, 25.2±6.3 and 63.0±0.3% for HPHT, DG and OG CVD diamond detectors, respectively. For measurements under light conditions alone using the tested detectors, the difference in response was > 5%, whereas in dark conditions the difference in response was < 3%. This signifies that once the diamond sensors are properly shielded from ambient light and their response stabilised, daily priming is not necessary;

(2) Given the importance of Fowler's dose rate linearity index Δ of solid-state detectors in radiation dosimtry, Δ was used as a relevant tool to identify a number of pertinent defect types which could influence the performances of the diamond detectors. Thermoluminescence emission was also identified as a suitable parameter that could be

utilised to probe the performances of diamond crystals. These findings suggest that diamond crystals could be selected or perhaps tailor-made with various defect levels which when used as sensing elements for dosimetric applications display optimum performance;

(3) Measurements of output factors under small-photon-field conditions demonstrated that an accuracy level within 3% could be achieved if the diamond detector size is ≤ 3/4 of field size, with the 'edge-on' orientation being an appropriate detector geometry for field sizes below 1x1 cm^2. In addition, the HPHT diamond sensors due to their low defect levels were found to show an overall better performance compared to the CVD crystals. A sensitivity value of 197.3 nC Gy^{-1} mm^{-3} was established with the probe using a HPHT diamond sensor in a radiation field of size 0.4x0.4 cm^2 compared to a value of 136.1 nC Gy^{-1} mm^{-3} obtained with a small-field diode detector;

(4) The dosimetric performances (i.t.o relative dose distributions, directional and dose rate response) of the diamond probe (using selected crystals as sensing elements) on exposure to various teletherapy beams were found to be in close agreement with data taken with reference dosimeters in the order of 1–2% with or without dose rate dependence corrections. Such performance was attributed to the near-tissue equivalence of the synthetic diamond probe and its low and stable background signal.

Overall, the study illustrated that differences in crystal quality due to the presence and influence of defect levels could cause a variation in the performances of various diamond sensors. Once a crystal is selected (based on the influence of defect levels) and coupled to the probe, then the near-tissue equivalent synthetic diamond probe could be used for clinical applications of various beam types in large as well as small radiation fields as demonstrated by the results of various dosimetric characterizations.

DEDICATION

This piece of work is dedicated to:

My parents

Tumasang M. Tabufor, of blessed memory (1923 – 2003)

and Julia Azah

My Brothers and sisters, and the entire Tabufor's family

And to all those who have inspired me through the advancement of scientific knowledge

ACKNOWLEDGEMENTS

First and foremost, I express gratitude to all those who have contributed towards the success of this project. A special acknowledgment goes to the Department of Science and Technology and National Research Foundation of South Africa through the Centre of Excellence in Strong Materials (CoE-SM) at the University of the Witwatersrand (Wits) for generously funding this project. Many thanks to the Division of Medical Physics at the Charlotte Maxeke Johannesburg Academic Hospital, and Radiation and Health Physics Unit at Wits which provided me with a conducive atmosphere to work on this project and for granting me the permission to utilize their radiation facilities.

Much credit goes to my supervisors, Professors Tom Nam and Trevor Derry, for their supervision, guidance, assistance and support which have made this piece of work what it is today. I am particularly grateful to Prof Nam, who introduced me in the field of diamond physics, design the radiation probe presented in this thesis and supervised the project in an exceptional manner. I started the project with very little idea on solid-state detector systems based on diamond, but with his guidance, encouragement and supervision, I developed the confidence, skills and knowledge to go through the project successfully. I am also thankful to Prof Derry, for the role he played to secure funding for me prior to the start of this research, and for his feedback and suggestions which have improved the readability of this thesis.

I would also like to thank the staff and postgraduate students in the School of Physics and CoE-SM at Wits for their positive criticisms and constructive ideas during seminar presentations. The assistance of the following individuals is acknowledged: Prof Michael Hayes, for preparing ohmic contacts on diamond surfaces; Prof J. van Wyk, for ESR measurements; Prof Jonathan Keartland, for useful discussions on ESR; Dr R. Erasmus, for Raman spectroscopy measurements; Mr Sikhumbuzo H. Mhlanga, who assisted with dosimetric setups; and Prof Debbie Van der Merwe, for valuable discussions on critical aspects in dosimetry. The Physics workshop, iThemba Labs and administrative staff in the CoE-SM are also acknowledged for technical assistance.

I would also like appreciate the spiritual and emotional supports and encouragement from my family and friends, especially my good friend, Siphephile Ncube.

Most of all I thank the Almighty God for His abundant love, grace and mercy.

CONTENT

CHAPTER ONE

INTRODUCTION

1.1 General introduction

Radiation describes the emission and propagation of energy from electromagnetic waves or energy propagated by moving subatomic particles with very high kinetic energy. This study is concerned with ionizing radiation (electrons, X- and gamma rays). By radiation detection properties as referred to in the title of this thesis, this study considers parameters that could influence the response of diamond to ionizing radiation. These include parameters such as the physical properties of diamond, imperfections (crystal defects and impurities), light sensitivity, crystal geometry or orientation, thermoluminescence (TL) emission and dark current. Furthermore, the term "medical applications" is limited to clinical radiation dosimetry.

1.2 Medical applications of ionizing radiation

The study and use of ionizing radiation in medicine started with the discovery of X-rays in 1895 by Wilhelm Roentgen followed by natural radioactivity by Henri Becquerel in 1896 and radium by Pierre and Marie Curie in 1898. The knowledge of the use of ionizing radiation in diagnosis and treatment of disease is now well established. Whereas diagnostic radiology and nuclear medicine employ ionizing radiation in the detection of cancer, radiotherapy describes the use of ionizing radiation in the treatment of cancer. Diagnostic procedures make use of low-energy X-rays (diagnostic radiology) and gamma rays (nuclear medicine) whereas in therapy, most commonly high-energy photon and electron beams in the megavoltage range are utilized. Radiotherapy employs two treatment methods – external beam radiotherapy (EBRT) and brachytherapy. Whilst EBRT is the term used to describe treatments in which the source of radiation is distant from the patient, brachytherapy describes treatments delivered at a short distance using radioactive sources or seeds placed either closed to or implanted within the target volume. The discussion in this thesis is limited to EBRT and mammography as both procedures cover the energy range often encountered in therapeutic and diagnostic radiology. In addition, EBRT is the common form of radiotherapy while screening mammography is done on a regularly basis (every one to two years).

1.3 X-ray Mammography

Breast cancer is the most common type of cancer among women. In the USA, it ranks second as a cause of cancer death in women (after lung cancer) (American cancer Society, 2014). It is estimated that 232,670 and 62,570 new cases of invasive and in situ breast cancer, respectively are expected to be diagnosed among women in the USA during 2014 with about

40,430 breast cancer deaths (40,000 women, 430 men) expected to occur (American cancer Society, 2014). Mammography is a radiographic imaging technique that employs low-energy X-rays to examine the human breast aimed at an early detection of breast cancer, typically through the detection of characteristic masses and/or micro-calcifications. X-ray mammography has been considered to be the most reliable, important and sensitive imaging technique currently available for early detection of breast cancer. Mammography is used for mass screening and for diagnostic examinations. Screening involves the examination of asymptomatic women with the intent of early detection of a breast lesion before it becomes palpable, whereas diagnostic mammography is performed on individuals who through physical findings and/or symptoms, may reveal that they have breast cancer.

A mammography X-ray machine (screen-film mammography) is usually operated in the energy range from 25 to 35 kVp and absorbed doses of the order of 1 to 2 mGy are measured (Klein et al., 1997). A higher radiation dose will normally lead to a better image contrast but this increases patient dose and may subsequently induce cancer in the radiosensitive breast as any exposure to ionizing radiation has a small but significant risk. The clinical X-ray beam used for mammography is produced when a beam of fast moving electrons from a cathode filament is rapidly decelerated in vacuum to collide and interact with a target material (anode) usually molybdenum. The X-ray machine is designed such that the X-ray beam produced is directed through an exit window to the exterior. A filter is usually inserted in the path of the X-ray beam to alter the beam quality by removing soft energy X-rays which do not contribute to image formation but increases patient dose. The filtered beam is then collimated to desired dimensions for breast imaging. A mammography unit is a dedicated unit in a diagnostic radiology department as the X-ray mammography machine is tailored to image only the breast. Compared to other diagnostic X-ray tubes (radiography, computed tomography (CT) and fluoroscopy) which usually use tungsten targets, molybdenum is a common anode material for screen-film mammography machines.

1.4 External beam radiotherapy (EBRT)

The main goal of radiotherapy is to deliver a high radiation dose (lethal dose) to the target volume while the surrounding normal tissues and organs at risk receive the lowest possible dose. Radiotherapy represents one of the three primary modalities for cancer management, the other two being chemotherapy (use of chemicals and drugs) and surgery. Sometimes, a combination of two or all three modalities is required for cancer management depending on

the stage of the disease and clinical decision. EBRT primarily applies megavoltage electrons (6–22 MeV) or X-ray photons (4–25 MV) from linear accelerators (linacs) or γ-ray photons from a teletherapy machine. Two γ-ray sources for teletherapy machines are ^{60}Co and ^{137}Cs but the former is widely used. A ^{60}Co teletherapy source emits two γ-ray energies at 1.17 and 1.33 MeV which constitute the useful therapy beam having, an average radiation energy of 1.25 MeV.

Megavoltage photons and electrons could be delivered with separate linacs, but modern linacs are capable of providing both photon and electron beams. The primary advantage of a modern linac over a ^{60}Co teletherapy unit is that a linac has a compact and efficient design that provides either a megavoltage X-ray or electron therapy beam with a wide energy range. The central axis depth-dose curve of an electron beam exhibits a high surface dose compared to megavoltage photon beams. Consequently, this feature provides electron beams a distinct clinical advantage over conventional X-ray modalities in the treatment of superficial tumours and lesions at shallow depths (< 5 cm deep) beneath the skin.

1.5 Clinical radiation dosimetry, effective atomic number and tissue-equivalence

Radiation dosimetry is the determination of the absorbed dose or some other physically relevant, related dosimetric quantity in a medium at a given point of interest. Usually these doses are determined with tissue-equivalent materials whose absorption characteristics are similar to those of human tissue (Yacoot et al., 1990). Tissue-equivalence therefore describes the property of a material to respond to radiation in an identical manner as the human body. Consequently to meet the requirements of a radiation dosimeter, the radiation sensing material and its holder ought to have absorption characteristics comparable to that of human tissue. As tissue-equivalence can be defined i.t.o effective atomic number (Z_{eff}) (Manohara et al., 2011), it implies that Z_{eff} of the dosimeter should be tissue equivalent. Z_{eff} is the atomic number of an element with which photons interact in a similar manner as with the given composite material (Khan, 2003). It represents the weighted average of the number of electrons per atom in a composite material (Manohara et al., 2008).

In radiation measurements, the Compton effect, photoelectric effect and pair production are the dominant interaction processes which play a role. The probability that a given process, called the interaction cross section, would take place with an attenuation material is a function of the atomic number Z of the absorbing medium and photon energy E.

Table 1.1: Approximate dependence of the interaction cross sections of Compton scattering, photoelectric effect and pair production as a function of Z and photon energy

Interaction process	Approximate dependence
Photoelectric Absorption (τ)	Z^4 for $E_p \leq 100$ keV
	Z^5 for $E_p \geq 3$ MeV
Compton scattering (σ)	Z
Pair production (κ)	Z^2 $E_p \geq 3.4$ MeV

Reference: Nam (1989)

For megavoltage photon beams in the clinical range, the Compton effect is the predominant mode of interaction (Khan, 2003). However in biological tissues, the absorption of relatively low-energy photons occurs principally by the photoelectric effect (Yacoot et al., 1990). A rough estimate for the probability of photoelectric absorption per atom over all ranges of photon energy E_p and Z is given by (Khan, 2003):

$$\tau = \text{constant} * (Z^n / E_p^{3.5}) \quad (1.1)$$

where the index n varies between 4 and 5 over E_p. Presented in Table 1.1 are the approximate dependence of the interaction cross sections for the Compton effect (σ), photoelectric effect (τ) and pair production (κ).

Since photoelectric absorption is the main mode of the interaction of low-energy photons with matter, it is essential to match the effective atomic number of radiation detectors to that of human tissue. Comparing diamond and silicon (as silicon is commonly used as a detector material) it is seen that the effective atomic number (Z_{eff}) values of 5.92, 7.42 and 7.64 for fats, muscle and lung, respectively closely match the atomic number of diamond (Z_C= 6) compared to silicon (Z_{Si} = 14) which matches bone (Z_{eff} =13.8) (Bampton, 1976; Yacoot et al., 1990). From the above it is clear that if Z_{eff} of the dosimeter is different to that of human tissue, the energy response of the dosimeter could vary significantly to the energy absorption in body tissue. Therefore, the energy dependence of a radiation detector for clinical dosimetry can be determined by comparing its atomic number to Z_{eff} of human tissue (Burgemeister, 1981). Consequently, for accurate measurement of radiation dose, the choice of the dosimetry systems should be limited to those which are tissue equivalent. The near-tissue equivalence of diamond therefore favours this unique mineral as a detector material. Hence, as a clinical radiation detector, it does not need significant energy correction factors to convert the

response to the actual deposited radiation dose since its energy response is similar it that of human tissue. Diamond does not only exhibit this remarkable attribute but other desirable properties that are attractive for medical applications.

1.6 Overview of absorbed dose measurements

The term absorbed dose, *D* is defined as (ICRU, 2011):

$$D = dE/dm \tag{1.2}$$

where, *dE* is the mean energy (in joules) imparted by ionizing radiation to a medium of mass dm (in kilograms). The SI unit for absorbed dose is the gray (*Gy*) defined as 1 *Gy* = 1 *J/Kg*.

The Spencer-Attix formulation (Spencer and Attix, 1955) of the famous Bragg-Gray cavity theory has been adopted by most International dosimetry protocols (AAPM TG-21, 1983; ICRU, 1984; AAPM TG-25, 1991; AAPM TG-51, 1999; IAEA TRS-398, 2000) for the measurement of absorbed dose. According to this theory, the magnitude of the ionisation signal produced by radiation in a small gas-filled cavity (gas or air as detector material) placed in a medium can be directly related to the absorbed radiation dose in the surrounding medium. A stringent requirement for the application of this theory is that the cavity should be sufficiently small so that the perturbation of the electron and photon fluences at the effective point of measurement, *P* is negligible. Based on the Spencer-Attix theory, the absorbed dose at point *P* in a medium (phantom)[1], D_{med} measured with a detector (det) can in general be expressed as:

$$D_{med} = R \cdot \left(\frac{\overline{L}}{\rho} \right)_{\text{det}}^{med} \cdot P_{pert} \tag{1.3}$$

where, R is the response of the detector (usually ionisation charge) corrected for various influenced factors such as ambient conditions, dose rate and directional dependence of the detector; 'det' represents the radiation sensing material of the detector (e.g. air, silicon or

[1] Dosimetric measurements are usually performed inside phantoms which simulate human tissue. Water is recommended as a reference phantom material since it is universally available and it closely approximates the radiation absorption and scattering properties of muscle and other soft tissues. Solid dry phantoms can be used as substitutes for water as water poses some practical problems (Khan, 2003).

diamond). The parameter $\left(\frac{\overline{L}}{\rho}\right)_{\text{det}}^{med}$ is the ratio of the average restricted mass collision stopping power[2] of the medium to the detector material which accounts for the change in the electron fuence at the point of measurement due to the insertion of the detector. The perturbation (P_{pert}) (or replacement, P_{repl} as referred to by AAPM (1983)) correction factor, corrects for perturbation in the photon and electron energy fluences at the point of measurement due to the introduction of the detector material in the medium (Khan, 2003). That is, it accounts for the spatial and angular variation of the radiation fluence in the detector and the surrounding medium (Björk et al., 2000). The perturbation correction factor depends on: the (i) detector material, that is, its size, Z_{eff} and density; (ii) beam energy and type; (iii) depth of measurement; and (iv) gradient of a depth-dose curve at the point of measurement (AAPM, 1983; Björk et al., 2000).

The factor P_{pert} which is required only if the detector perturbs the relationship between D_{med} and R has two components, the fluence, P_{fl} and gradient, P_{gr} correction factors for measurements made under conditions of electronic equilibrium (Khan, 2003). That is,

$$P_{pert} = P_{fl} \cdot P_{gr} \tag{1.4}$$

For measurements made with ion chambers for instance, P_{fl} is the ratio of electron fluences with and without (cavity is filled with surrounding medium) the cavity. When the measurement of electron fluence is performed with a cylindrical chamber, there is an upstream shift in the effective point of measurement depending on the radius of the air cavity. As a result, the measured ionization is greater than that if there was no shift or if the cavity radius was zero. Therefore, P_{gr} is the component of P_{pert} caused by a shift in the point of measurement of a detector. Its magnitude depends on dose gradient and detector size.

The factors $\left(\frac{\overline{L}}{\rho}\right)_{\text{det}}^{med}$ and P_{pert} are both energy dependent, so $\left\{\left(\frac{\overline{L}}{\rho}\right)_{\text{det}}^{med} \cdot P_{pert}\right\}$ in general represents the energy dependence of the detector (Van der Merwe and Keddy, 1999). In fact this energy-dependent term is used to convert depth ionization curves to depth-dose curves if

[2] The term stopping power refers to the energy loss by electrons per unit path length of a material (Khan, 2003).

the response of the detector is dependent on beam energy. This indicates that a tissue-equivalent detector is necessary for the accurate measurements of absorbed dose since its response will not vary with beam energy. It can therefore been seen that ionization measurements taken with a tissue-equivalent detector such as diamond could be used directly as absorbed dose data to tissue without energy dependent correction factors unlike measurements taken with energy dependent dosimeters such as air ionization chambers.

Silicon diodes are well-known to show significant energy dependence at lower electron and photon (≤ 100 keV) energies (Vatnisky and Järvinen, 1993; Rustgi, 1998) due to the non-tissue equivalence of diode detectors. Illustrated in Fig. 1.1 are the mass collision stopping-power ratios for water-to-carbon and water-to-silicon as a function of electron energy (water is a reference medium used in clinical dosimetry). A correction for the change in stopping-power ratio of water-to-silicon with electron energy would significantly improve dosimetric data taken with silicon diode detectors, especially at energies below 5 MeV. The water-to-carbon stopping-power ratio is almost constant with electron energy over the range 1–20 MeV, which is an advantage for diamond detectors over diodes and air ion chambers.

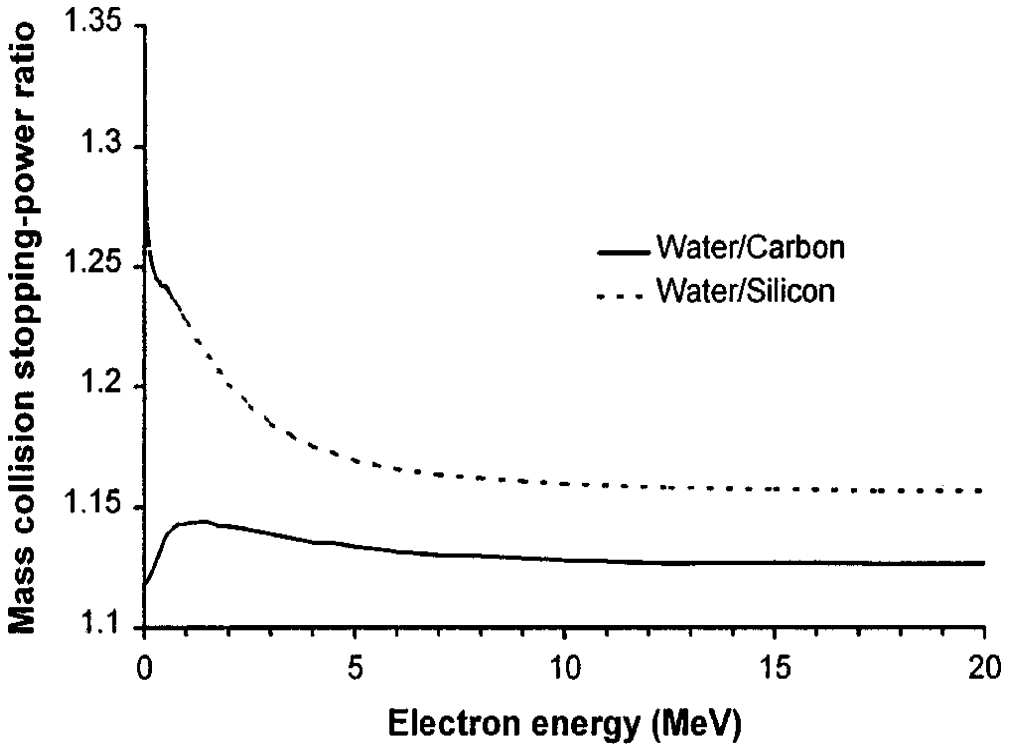

Figure 1.1: Mass collision stopping-power ratios for water-to-silicon and water-to-carbon as a function of electron energy References: (Björk et al., 2000; ICRU, 1984).

1.7 An overview of the calibration of high-energy photon and electron beams

Prior to clinical use, the output of electron and photon beams generated by radiation machines is usually calibrated. Beam calibration (reference dosimetry) is the determination of absorbed radiation dose in reference irradiation conditions (Podgorsak, 2005). It ensures optimization and accurate delivery of prescribed dose to patients. Dosimetry protocols recommend that the calibration of photon and electron beams be performed in a water phantom with dimensions of at least 30 x 30 x 30 cm^3. Furthermore, water is the material to which the dose calibration is referenced. The TG-21 protocol (AAPM, 1983) however recommends that plastic phantoms (polysterene or Perspex) may be used in addition to water, but with the requirement that the dose calibration be referenced to water. Thus 'medium' as used in section 1.5 refers to the type of phantom material employed.

For the dosimetry of photon beams, if the spectral distribution and fluence of photons (primary and scattered) at a given point of measurement in plastic are the same as at a comparable point in water, the dose to water is related to the dose to plastic by:

$$D_{water} = D_{plastic} \cdot \left(\frac{\overline{\mu}_{en}}{\rho} \right)_{plastic}^{water} \tag{1.5}$$

where, $D_{plastic}$ is the dose to plastic and $\left(\frac{\overline{\mu}_{en}}{\rho} \right)_{plastic}^{water}$ is the ratio of the mean mass energy absorption coefficient of water to that of plastic. In the case of electron beams if dose is measured in a plastic phantom at the depth of dose maximum, d_{max} (depth of peak absorbed dose), then the dose to water is given by:

$$D_{water} = D_{plastic} \cdot \left(\frac{\overline{S}}{\rho} \right)_{plastic}^{water} \cdot \Phi_{plastic}^{water} \tag{1.6}$$

where, $\left(\frac{\overline{S}}{\rho} \right)_{plastic}^{water}$ is the average unrestricted mass collision stopping power ratio of water to plastic and $\Phi_{plastic}^{water}$ is the ratio of the electron fluence at d_{max} in water to that of plastic. In Equations (1.5) and (1.6), $D_{plastic}$ is given by Eq. (1.3) as the dose to medium.

Since in medical radiation dosimetry the dose to soft tissue (or muscle) is the quantity of interest, it is essential to convert dose to water, D_{water} to dose to tissue, D_{tissue} whenever dose is specified for patient treatment. These two quantities are related by (Khan, 2003):

In the case of photon beams,

$$D_{tissue} = D_{water} \cdot \left(\frac{\overline{\mu}_{en}}{\rho} \right)_{water}^{tissue} \tag{1.7}$$

For electron beams,

$$D_{tissue} = D_{water} \cdot \left(\frac{\overline{S}}{\rho} \right)_{water}^{tissue} \tag{1.8}$$

where $\left(\frac{\overline{\mu}_{en}}{\rho} \right)_{water}^{tissue}$ and $\left(\frac{\overline{S}}{\rho} \right)_{water}^{tissue}$ are the ratios of the average mass energy absorption coefficient and unrestricted mass collision stopping power of tissue to water, respectively.

1.8 Overview of dosimetry in mammography

The objective of dosimetry is principally to evaluate the risk of radiation-induced carcinogenesis in mammography procedures. Three dosimetric quantities are used in mammography (IAEA TRS 457, 2007): the incident air kerma, K_i; the entrance surface kerma, K_e and the mean absorbed dose to the glandular tissue within the breast, called the mean glandular dose, D_G which is of primary interest as it is the risk related parameter. The risk assessment quantity (D_G) is not measured directly but it can be determined from measurements of the incident air kerma to a 4 cm thick breast substitute phantom using a conversion coefficient (Dance, 1990). The approach involves the determination of K_i to the breast substitute phantom (measured without backscatter) and the half value layer (HVL) of the X-ray set. The incident air kerma is determined from the product of tube loading (exposure time-current product, mAs) and machine output (air kerma per mAs) with the phantom removed (Assiamah, 2004).

Using Perspex (also known as polymethyl methacrylate or PMMA) as breast substitute phantom the mean glandular dose can be estimated as: (Dance, 1990; Dance et al., 1999):

$$D_G = K_i\, p\, g \tag{1.9}$$

where K_i is the incident air kerma at the surface of the breast without backscatter; p is a factor that converts the incident air kerma to the PMMA phantom to that of the standard breast and g is the conversion coefficient that converts the incident air kerma for the standard breast to mean glandular dose. It is recommended that the diagnostic dosimeter (usually a calibrated ion chamber) used for X-ray output measurements should have a flat energy response over the mammographic kilovoltage (kV) range (Dance et al., 1999).

1.9 Rationale and aim of study

Radiotherapy aims at delivering a lethal radiation dose to malignant tissues in order to provide a high probability of tumour control while sparing or inducing minimal damage to adjacent normal tissues. As a result radiotherapy is directed towards keeping normal tissue complications within acceptable limits while attaining a high therapeutic ratio, i.e., the ratio of tumour control probability (TCP) to normal tissue complication probability (NTCP) (Bampton, 1976). Also, as screening mammography involves the examination of potentially healthy individuals unlike radiotherapy where the clinical objective is to eradicate a disease, the risk of the procedure has to be carefully balanced against the benefits as any exposure to ionizing radiation has a small but non-negligible risk of radiation-induced carcinogenesis. Consequently, accurate medical radiation dosimetry is essential to the success of diagnostic and therapeutic procedures.

Dosimetry deals with techniques for the quantitative determination of absorbed dose in a given medium by ionizing radiation (Podgorsak, 2005). It represents one of physical procedures aimed at achieving the overall ICRU (1976) ±5% uncertainty of absorbed dose delivery in radiotherapy. The goal of clinical dosimetry is to acquire and evaluate essential beam parameters with a high degree of accuracy in order to assess the absorbed dose to the human tissue. Of particular relevance is the fact that compared to measurements in large or classical (> 4 x 4 cm^2) radiation fields, an extra degree of accuracy is required for the dosimetry of small fields (≤ 4 x 4 cm^2) as a result of the loss or absence of lateral electronic equilibrium in small fields (Haryanto et al., 2002; Lee et al., 2012; Wuerfel, 2013). To achieve the highest possible accuracy especially for measurements in small radiation fields, three

essential properties are required of radiation detectors: tissue-equivalence of the detector material including its encapsulation; high spatial resolution and high radiation sensitivity.

However, the state-of-the-art detectors (air ion chambers and silicon diodes) frequently used for the clinical dosimetry of electron and photon beams have a range of applicability limited by the design and inherent properties of their respective detector materials (Heydarian et al., 1993). Whereas large-size ion chambers are not appropriate for high spatial resolution measurements due to the volume averaging effect (Haryanto et al., 2002; Lee et al., 2012; Wuerfel, 2013), the use of ion chambers with very small physical sizes leads to extremely low sensitivity to radiation because of the low density of air (Heydarian et al., 1993). Diode detectors have high spatial resolution and are highly sensitive to radiation as a result of the high density of silicon compared to air, but they have a major drawback of being non-tissue equivalent (Heydarian et al., 1993; Björk et al., 2000). Consequently, diode detectors show an over-response in both large (Westermark et al., 2002) and small fields (Haryanto et al., 2002; Laub and Wong, 2003). Furthermore, the energy and air density dependence of air ion chambers, the directional dependence of parallel-plate chambers and silicon diodes (Brahme, 1985) and the use of separate shielded and unshielded diodes for photon and electron beam dosimetry, respectively (Heydarian et al., 1993) are some of the drawbacks.

In contrast, diamond is a potential detector material for dosimetric applications due to its unique properties. Additionally, a single probe with synthetic diamond as the radiation sensing element could be used for both photon and electron beams dosimetry in large as well as in small and very small ($< 1 \times 1$ cm^2) radiation fields. By virtue of its near-tissue equivalence; the high solid-state to air density ratio, which is of the order of 3.0×10^3 (Bruzzi et al., 2000); and with an atomic number density of 1.75×10^{23} atoms cm^{-3} (Mainwood, 2000) which corresponds to a molar volume of 3.44 cm^3 mol^{-1}(Assiamah et al., 2007) diamond detectors with small physical sizes can be constructed for high spatial resolution measurements which is an advantage over large volume and non-tissue equivalent detectors.

However, the application of diamond detectors for medical dosimetry is still limited by various challenges often encountered in the field which hinder both dosimetric performance and the availability of the product. Some pertinent challenges include: ease of fabrication and compatibility with commercially available electrometer systems; encapsulation and positional uncertainties due to detector geometry; dark currents or background signals which are

undesirable sources of noise in radiation measurements; the instability of response of diamond detectors needing daily priming; the dose rate dependence of diamond detectors in relative dosimetry; directional dependence and cable irradiation effects; and crystal selection. In addition, the relationship between crystal size and field size for small-field dosimetry has not been investigated and only a few studies (Ciacaglioni et al., 2012; Marsolat et al., 2013) have evaluated the performance of a synthetic diamond detector of a particular type under small-field conditions.

By exploring the radiation detection properties of synthetic diamond crystals of various types aimed at addressing the above challenges in order to improve dosimetric accuracy, this thesis investigates the possibility of utilising a single synthetic diamond probe for the dosimetry of low-energy diagnostic X-rays and high-energy radiotherapy beams in large as well as in small radiation fields. The dosimetric performances of examined crystals were correlated to material characteristics (defects and impurity levels).

1.10 Thesis outline

With the overall aim of improving dosimetric accuracy, this thesis explores the possibility of developing a multi-purpose radiation probe with synthetic diamond as the sensing material for the dosimetry of mammography X-rays and radiotherapy beams (megavoltage photons and electrons) under broad and small field conditions. The thesis is structured by publications (chapters 4 to 8), which is allowed at the University of the Witwatersrand. Consequently, there will be repetition but I have tried as much as possible to limit it.

Chapter 2 gives a description of the crystal structure of diamond including its properties and diamond type classification. The principle of operation of a diamond radiation detector and an overview of dosimetry with diamond are presented including the challenges in the field.

Chapter 3 presents the synthetic diamond crystals examined in this thesis and the characterization techniques which include: Raman spectroscopy; Electron spin resonance (ESR); Fourier transform infra-red spectroscopy (FTIR) and thermoluminescene (TL) emission. These techniques were conducted to assess and compare crystal quality and to correlate crystal quality with dosimetric performance. For the characterized crystals, only one Raman spectrum (as well as ESR and FTIR) is shown as all the spectra for each technique

show similar features but of different sizes. A prototype design of the multi-purpose synthetic diamond probe is also presented together with irradiation measurements.

In chapter 4, preliminary dosimetric measurements to determine whether the synthetic diamond probe has been optimized (i.t.o of various influencing quantities) for the evaluation of detector performances clinical conditions are presented. The measurements were taken with mammography X-rays and megavoltage electrons.

Presented in chapter 5 is an evaluation of some pertinent parameters that influence the dosimetric performance of synthetic diamond detectors. Parameters such as: the unstable response of diamond detectors requiring priming is systematically studied using mammography X-rays; the angular dependence and the influence of dose rate dependence correction factor in relative electron dosimetry are evaluated.

Chapter 6 presents a systematic study of the dose rate dependence of synthetic diamond detectors in relative therapy electron dosimetry. The aim here was to select a suitable crystal for small-field electron dosimetry.

In chapter 7, the influence of defect levels on the dose rate dependence of synthetic diamond detectors of various types on exposures to high-energy radiotherapy beams is presented. The dependence of the dose rate linearity index on bias voltage, defect levels, beam energy and type is systematically investigated.

Chapter 8 investigates the relationship between detector size and field size under small-photon field conditions using synthetic diamond crystals as sensors. The aim was to select a suitable crystal type and size for small-field dosimetry.

A general discussion of the results of the study and conclusions based on the major findings are presented in chapter 9.

Outlined in Appendix A is an evaluation of the performance of the synthetic diamond probe on exposure to ^{60}Co radiation, a justification of 2% accuracy for the influence of Fowler's dose rate linearity index in relative dosimetry is presented in Appendix B, and a list of publications, patents and conference presentations is provided in Appendix C.

References

AAPM TG-21, 1983. A protocol for the determination of absorbed dose from high energy photon and electron beams. *Med. Phys.* **10**, 741.

AAPM TG-25 1991. Clinical electron beam dosimetry. *Med. Phys.* **18**, 73.

AAPM TG-51, 1999. Protocol for clinical reference dosimetry of high-energy photon and electron beams. *Med. Phys.* **26**, 1847.

American Cancer Society. *Cancer Facts & Figures 2014*. Atlanta: American Cancer Society; 2014.

Assiamah, M., 2004. Dosimetric techniques for mammography mass screening programs. *PhD Thesis, University of the Witwatersrand, Johannesburg***.**

Assiamah, M., Nam, T.L., Keddy, R.J., 2007. A synthetic diamond probe for low-energy X-ray dose measurements. *Appl. Radiat. Isot.* **65**, 545.

Bampton, F.K., 1976. A medical application for radiosensitive diamonds. *Ind. Diamond Rev.* **36,** 55.

Björk, P., Knöös, T., Nilsson, P., 2000. Comparative dosimetry of diode and diamond detectors in electron beams for intraoperative radiation therapy. *Med. Phys.* **27**, 2580.

Brahme, A., 1985. Correction for the angular dependence of a detector in electron and photon beams. *Acta Radiol. Oncology*. **24**, 301.

Bruzzi, M., Bucciolini, M., Cirrone, G.A.P., Cuttone, G., Mazzocchi, S., Pirollo, S., Sciortino, S., 2000. Characterisation of CVD diamond dosimeters in on-line configuration. *Nucl. Instrum. Methods Phys. Res*. A **454**, 142.

Burgemeister, E.A, 1981. Dosimetry with a diamond operating as a resistor. *Phys. Med Biol*. **26**, 269.

Ciancaglioni, I., Marco Marinelli, Milano, E., Prestopino, G., Verona, C., Verona-Rinati, G., 2012. *Med. Phys.* **39**, 4493.

Dance, D.R., 1990. Monte Carlo calculation of conversion factors for the estimation of mean glandular breast dose. *Phys. Med. Biol.* **35**, 1211.

Dance, D.R., Skinner, C.L., Carlsson, G.Alm, 1999. Breast dosimetry. *Appl. Radiat. Iso*. **50**, 185.

Garcia, M., Jemal A, Ward, E.M., Center, M.M., Hao, Y., Siegel, R.L., Thun, M.J. *Global Cancer Facts & Figures 2007*. Atlanta, GA: American Cancer Society, 2007.

Haryanto, F., Fippel, M., Laub, W., Dohm, O., Nüsslin, F., 2002. *Phys. Med. Biol*. **47**, N133.

Heydarian, M., Hoban, P.W., Beckham, W.A., Borchardt, I.M, Beddoe, A.B., 1993. Evaluation of a PTW diamond detector for electron beam measurements. *Phys. Med. Biol*. **38**,

1035.

IAEA International Atomic Energy Agency. *Dosimetry in Diagnostic Radiology: An International Code of Practice*. TRS 457, IAEA, Vienna, 2007.

IAEA International Atomic Energy Agency. *Absorbed Dose Determination in External Beam Radiotherapy: An International Code of Practice for Dosimetry based on Standards of Absorbed Dose to water*. TRS-398, IAEA, Vienna, 2000.

ICRU *International Commission on Radiation Units and Measurements. Determination of Absorbed dose in a Patient Irradiated by Beams of X or Gamma rays in Radiotherapy Procedures.* ICRU Report 24, Bethesda, 1976.

ICRU International Commission on Radiation Units and Measurements. Radiation dosimetry: Stopping powers for electrons and positrons. Report No. 37, ICRU, Bethesda, MD, 1984.

ICRU *International Commission on Radiation Units and Measurements. Fundamental Quantities and Units for Ionizing Radiation (Revised). Journal of ICRU*, **11** Report 85, 2011.

Khan, F.M. The Physics of Radiation Therapy, 3rd ed. Philadelpia: Lippincott & Wilkins, 2003.

Klein, R., Aichinger, A., Dierker, J., Jansen, J.T.M., Joite-Barfuß, S., Säbel, M., Schulz-Wendtland, R., Zoetelief, J., 1997. Determination of average glandular dose with modern mammography units for two large groups of patients. Phys. Med. Biol. **42,** 651.

Laub, W.U., Wong, T., 2003. The volume effect of detectors in the dosimetry of small fields used in IMRT. *Med. Phys.* **30**, 341.

Lee, S. H., Kim, J., Nam, Y. S., Cho SamJu, Kwon, S., Lee, S., Shim, J.B., Kim, C.Y., Min, C.K., Cho, K.H., Huh, HyunDo, 2012. Analysis of Output Factors with Various Detectors in Small-field Electron-beam Radiotherapy. *Journal of the Korean Physical Society*, **60**, 875.

Mainwood, A., 2000. Recent developments of diamond detectors for particles and UV radiation. *Semicond. Sci. Technol.* **15**, R55.

Manohara, S.R., Hanagodimath, S.M., Thind, K.S., Gerward, L., 2008. On the effective atomic number and electron density: A comprehensive set of formulas for all types of materials and energies above 1 keV. *Nucl. Instrum. Methods Phys. Res.* B **266**, 3906.

Manohara, S.R., Hanagodimath, S.M., Gerward, L., 2011. Energy absorption buildup factors of human organs and tissues at energies and penetration depths relevant for radiotherapy and diagnostics. *Journal of Applied Clinical medical Physics*, **12**, 296.

Marsolat, F., Tromson, D., Tranchant, N., Pomorski, M., Le Roy, M., Donois, M.,

Moignau, F., Ostrowsky, A., De Carlan, L., Bassinet, C., Huet, C., Derreumaux, S., Chea, M., Cristina, K., Boisserie, G., Bergonzo, P., 2013. *Phys. Med. Biol*. **58**, 7647.

Nam, T.L., 1989. Nuclear radiation detection properties of diamond. *PhD Thesis, University of the Witwatersrand, Johannesburg*.

Podgorsak, E.B. *Radiation Oncology Physics*: A Handbook for Teachers and Students, IAEA, Vienna, 2005.

Rustgi, S.N., 1998. Application of a diamond detector to brachytherapy dosimetry. *Phys. Med. Biol.* **43**, 2085.

Spencer, L.V., Attix, F.H., 1955. A theory of cavity ionization, *Radiat. Res.* **3**, 239.

Van der Merwe, D.G., Keddy, R.J., 1999. Relative electron dosimetry using a synthetic diamond probe. *Radiat. Phys. Chem.* **54**, 325.

Vatnisky, S., Järvinen, H., 1993. Application of a natural diamond detector for the measurement of relative dose distributions in radiotherapy. *Phys. Med. Biol.* **38**, 173.

Westermark, M., Arndt, J., Nilsson, B., Brahme, A., 2000. Comparative dosimetry in narrow high-energy photon beams. *Phys. Med. Biol.* **45**, 685.

Wuerfel, J.U., 2013. Dose measurements in small fields. *Med. Phys. Int. J.* **1**, 82.

Yacoot, A., Moore, M., Makepeace, A., 1990. X-ray studies of synthetic radiation-counting diamonds. *Phys. Med. Biol.,* **35**, 1409.

CHAPTER TWO

HISTORICAL BACKGROUND AND LITERATURE REVIEW

2.1 Crystalline structure and physical properties of diamond

The structure of a material determines its properties such as physical, mechanical, electrical, chemical and optical properties, and eventually determines its industrial applications. For instance, diamond and graphite are two universally known allotropes of carbon, but they differ in structure by bonding types and arrangement of atoms. Whereas diamond is the cubic form of crystalline carbon of extreme hardness and the carbon atoms in a pure diamond lattice are covalently bonded with sp^3 hybridised bonds in a tetrahedral structure, graphite is soft, has sp^2 bonds and a hexagonal structure (Kalish, 2007). Consequently, diamond serves as an abrasive material while graphite is commonly used as a lubricant. The crystalline structure of diamond is described by the cubic unit cell of the diamond lattice as illustrated in Fig. 1. The distance between neighbouring atoms is 0.15 nm and the diamond lattice has a face-centred cubic (FCC) structure (Ziman, 1972; Cazaferri and Rytz, 1996).

Carbon (Z_C = 6), silicon (Z_{Si} = 14) and germanium (Z_{Ge}= 32) are Group IV elements of the Periodic Table (PT). Although Si and Ge are commonly used as semi-conductor materials for the fabrication of electronic devices and sensors, pure diamond being an insulator has several exceptional properties suitable for industrial applications compared to both silicon and germanium. Listed in Table 1 are some of the unique properties of diamond compared to those of silicon. Other outstanding properties of diamond include its: high radiation hardness (due to the high density of strong bonds in the crystal lattice); chemical inertness, which

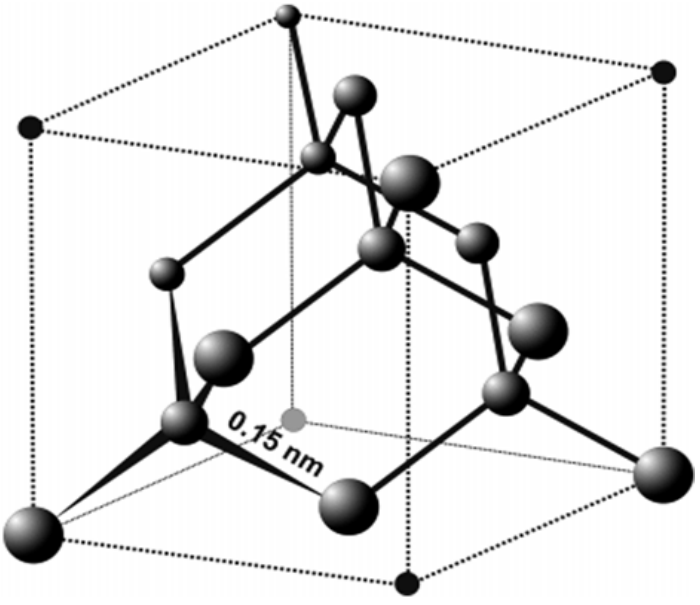

Figure 2.1: Basic cubic structure of diamond. Reference: (Gracio et al., 2010)

Table 2.1: Some properties of diamond compared to silicon at 293 K.

Property	Diamond	Silicon
Mass density (g cm^{-3})	3.515	2.33
Atomic density (cm^{-3})	1.75×10^{23}	4.83×10^{22}
Band gap (eV)	5.47	1.12
Resistivity (Ω.cm)	$>10^{12}$	2.3×10^{5}
Breakdown voltage (V cm^{-1})	10^{7}	3×10^{5} (p-n junction)
Electron mobility, μ_e (cm^2 V s^{-1})	2400	1350
Hole mobility, μ_h (cm^2 V s^{-1})	2100	480
Saturation velocity, v_s (km s^{-1})	220	82
Dielectric constant	5.7	11.9
Energy to form e–h pair, ε (eV)	13	3.6
Thermal conductivity (W m^{-1} K^{-1})	~2000 (max)	150

Reference: Mainwood (2000)

makes it suitable for operations in harsh environments where silicon can not operate; non-toxicity, which makes it suitable for in vivo dosimetry; high sensitivity to radiation (due to its high mass density) and stability of response; extreme mechanical hardness (~ 100 GPa); low leakage current and a good time resolution; and near-tissue equivalence due to its low atomic number which matches closely the effective atomic number of human soft tissue (Z_{eff} = 7.4) (Mainwood, 2000; Kania, 1993; Manfredotti et al., 1998; Whitehead et al., 2001; Guerrero et al., 2004; Cirrone et al., 2006; Gracio et al., 2010). This last property offers diamond a distinct advantage over silicon for applications in clinical dosimetry.

2.2 Electronic band structure of diamond

The band model of solids which, describes electron energies and their distributions determines the type of solid and its macroscopic properties (Ziman, 1972). It can provide a basic explanation for the electrical properties of solids. As Fig. 2.2 demonstrates, an insulator such as diamond is described by the band model as a solid material characterized by a relatively wide band gap. In the case of pure diamond (an indirect band gap material), the band gap is about 5.47 eV. The valence band which lies below the energy band gap is

completely occupied by electrons whereas the conduction band (above the energy gap) is devoid of electrons. As the electrons in the valence band are not free to move through the crystal lattice, no electric signal can flow, hence diamond is an insulator at room temperature. If however an electron in the valence band acquires sufficient energy (e.g. thermally or when the material is irradiated) such that it is excited from the valence band to the conduction band, it becomes free to move as does the hole created in the valence band. Due to the large band gap, about 5.47 eV of energy is required to excite an electron from the valence band to the conduction band, compared to 1.12 eV for silicon and 0.7 eV for germanium. Consequently, pure diamond is a wide band gap material, as 5.47 eV is higher than the thermal energy k_BT ~ 0.025 eV (where k_B is the Boltzmann's constant and T is the absolute temperature) and the probability of thermal excitation of an electron from the valence band to the conduction band is negligible at room temperature (Gracio et al., 2010).

As shown Fig. 2.2, the presence of defects and impurities (imperfections) in the diamond lattice may create electronic levels in the band gap **(**Kalish, 2007) which could alter the electrical performance of the material. Crystal imperfections can trap charge carriers, resulting in reduced sensitivity or may dope the crystal making it a semiconductor. An electron trap would temporarily capture an electron with subsequent thermal release to the conduction band whereas a hole trap would momentarily capture a hole and later release it thermally to the valence band. The time between the capture and thermal release of charge carriers depends on the temperature of the crystal and the trapping energy levels. Instead of acting as trapping centres, some impurities would act as recombination centres causing the

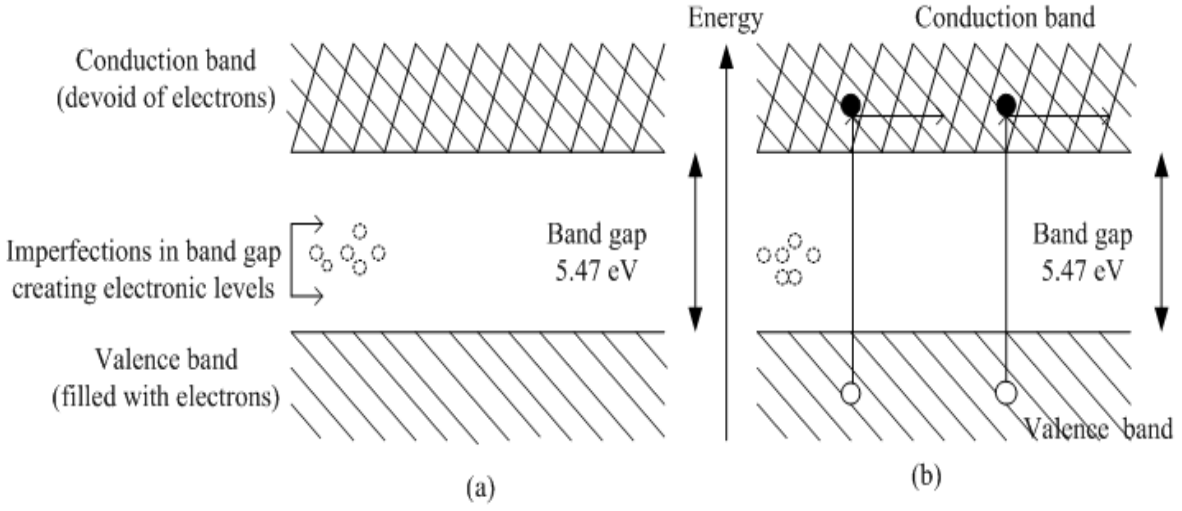

Figure 2.2: Electronic band structure of diamond illustrating ground (a) and excited (b) states

recombination of a free electron and a hole. The mechanism of recombination depends on the nature of the recombination centre – recombination could either take place between an electron and a free hole captured at the recombination centre or between a hole and a free electron captured at the recombination centre. In either case, the outcome is the same. Although both trapping and recombination centres result in reduced signal, the process of trapping is temporary while charge is completely lost in the process of recombination and energy is usually released. The released energy could take the form of a photon (radiative recombination) or a phonon (non-radiative recombination). In the former case, if the photon is released in the visible region of the electromagnetic spectrum as is usually the case the recombination centre is known as a luminescent centre. In the latter case which is an alternative to radiative recombination, the energy liberated in the form of phonons increases the temperature of the crystal although the temperature increase may not be detectable.

2.3 Classification of diamond

Diamond could be natural or synthetic. There are various processes which crystallize carbon to the diamond structure. While the natural genesis of diamond takes place in the earth's crust, synthetic diamond crystals are basically produced by the high-pressure, high-temperature (HPHT) and chemical vapour deposition (CVD) processes. At room temperature, graphite is the stable form of carbon whereas diamond is the metastable form so the natural genesis of diamonds occurs in the region where diamond is thermodynamically stable as illustrated in the carbon phase diagram in Fig. 2.3 (Balmer et al., 2009). The growth of synthetic diamond by the HPHT method basically converts graphite to diamond by applying appropriate temperature and pressure conditions in the thermodynamically stable region. The use of various transition metals (e.g. Co, Ni and Fe) as solvents and catalysts is essential in the synthesis of HPHT diamonds (Yacoot et al., 1990). The growth of diamond by the CVD process involves the deposition of carbon atoms that originate from the dissociation of a carbon-containing gas precursor on a solid substrate (Gracio et al., 2010; Balmer et al., 2009). As this process is in the region where diamond is metastable compared to graphite, diamond synthesis under CVD conditions is driven by kinetics and not thermodynamics (Balmer et al., 2009). If the solid substrate or seed is bulk diamond (natural or synthetic) the resulting films are said to be homo-epitaxial or single crystalline as opposed to hetero-epitaxial or polycrystalline films which are deposited on non-diamond substrates (Gracio et al., 2010, Balmer et al., 2009). So CVD diamond can either be single crystal or polycrystalline (usually grown on Si substrates (Kalish, 2007).

In Period 2 of the Periodic Table carbon (Z_C = 6) is located between boron (Z_B = 5) and nitrogen (Z_N = 7) which are commonly observed impurities in diamond (Walker, 1979). The classification system of diamond is based solely on the presence or absence of N and B impurities (and their configurations) in the diamond lattice as illustrated in Fig. 2.4 (Breeding and Shigley, 2009). Pure diamond would be made up of only carbon atoms arranged in a regular pattern in the diamond lattice. However, N and B atoms often replace some C atoms in the diamond lattice. Nitrogen is frequently observed in natural diamonds and its presence indicates that it is usually involved during its growth. Diamond type classification divides diamonds into two groups as Type I or Type II (Breeding and Shigley, 2009). Type I diamonds contain sufficient and detectable amounts of N impurities while Type II diamonds contain the least (or no measurable) N impurities.

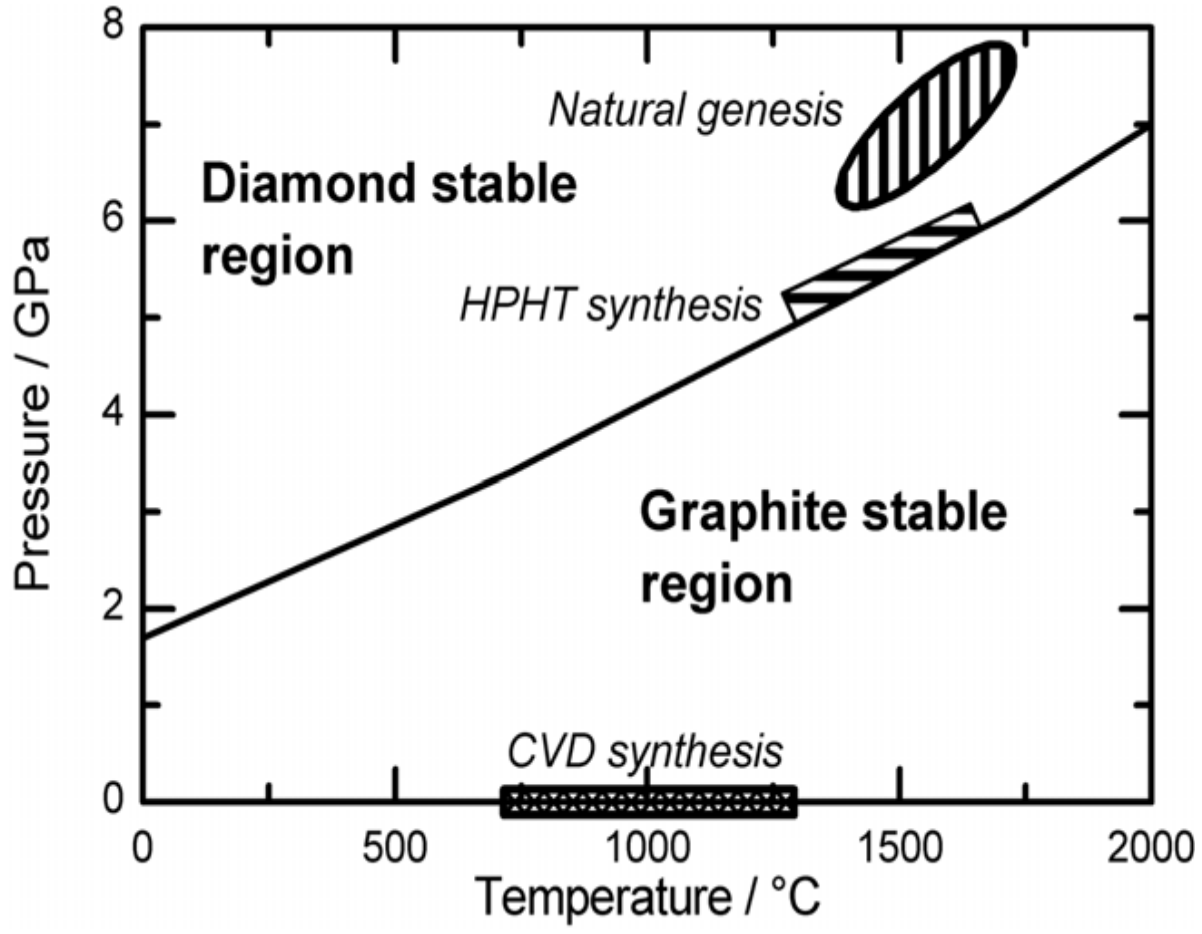

Figure 2.3: Carbon phase diagram indicating the main regions where diamond growth occurs. Reference: Balmer et al. (2009).

As demonstrated in Fig 2.4, both Types I and II have sub-divisions as follows:

Type Ia This category of diamonds contains aggregated N impurities. Type Ia diamonds are sub-divided into Type IaA and Type IaB. Type IaA contains the A-aggregate of N, which consists of a pair of N atoms. Type IaB contains the B-aggregate, which is comprised of four N atoms surrounding a vacancy. A- and B-aggregates of N can be identified by infra-red absorption spectroscopy.

Type Ib This set of diamonds contains N impurities predominantly as single substitutional or isolated N atoms. Their concentration can be measured accurately by electron spin resonance (ESR) method.

Type IIa This class of diamonds usually contains no measurable impurities of any kind.

Type IIb This group contains boron impurities and has semiconducting (p-type) properties.

It is well known that due to the varied geological histories of natural diamonds, their composition and properties vary considerably (Benabdesselam et al., 1999; Balmer et al., 2009).

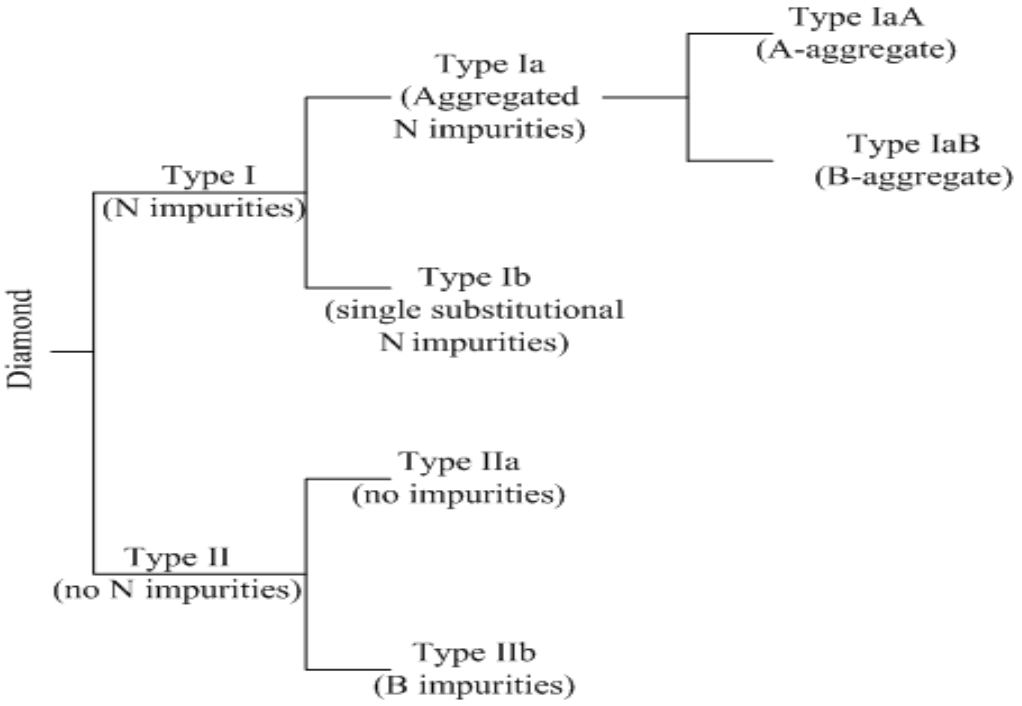

Figure 2.4: Diamond type classification system is based on the presence or absence of N and B impurities and their arrangements in the diamond lattice. Reference: Breeding and Shigley (2009).

Table 2.2: Characteristic colours of natural diamonds according to diamond type

Diamond Type	Impurity	Most common colours
Ia	Aggregated N	Colourless, brown, yellow, pink Orange, green, violet
Ib	Isolated N atoms	Yellow, orange, brown
IIa	None	Colourless, brown, pink, green
IIb	Boron	Blue, grey

The growth of diamond synthetically therefore offers a significant degree of control over the quality and geometry of the diamond obtained as crystals with reproducible properties can be produced compared to natural growth. Most natural diamonds are of type Ia while synthetic diamonds are mostly of type Ib.

2.4 Link of diamond type to colour and sequence of nitrogen aggregation in diamond

Natural diamonds usually show colours that correlate to their diamond type as illustrated in Table 2.2 and Fig. 2.5. For instance, type Ib diamonds are yellow, brown and orange in colour (Breeding and Shigley, 2009).

Figure 2.5: Colour of diamond is strongly influenced by the types of imperfection in the diamond lattice. As a result, diamond type plays an important role in the potential colours of natural, synthetic, and treated stones. Reference: Breeding and Shigley (2009)

As discussed in detail by Taylor et al. (1990), the sequence of N aggregation in diamond begins with isolated N atoms (N_s) aggregating to form the more stable A-aggregates. Further aggregation leads to the formation of B-aggregates. Associated with B-aggregate formation is the simultaneous production of larger planar structures called platelets. A side reaction in the A → B aggregation process produces N3 centres. Platelets degrade to form a diamond with pure B character or may undergo catastrophic degradation, resulting in the formation of platelet-depleted diamonds containing mixed A- and B-aggregates (Woods, 1986). Platelet-depleted diamonds have been termed irregular diamonds by Woods (1986).

2.5 Mechanism of operation of a diamond radiation detector

At room temperature, pure diamond is an insulator with a carrier concentration of about 10^{-28} carriers/cm^3 compared to ≈ 10^{10} and ≈ 10^{14} carriers/cm^3 for Si and Ge, respectively (Bampton, 1976). Nonetheless, when ionizing radiation interacts with diamond, electron-hole pairs (charge carriers) are generated. To acquire these carriers, it is essential to apply an external bias voltage to electrical (ohmic) contacts usually produced on opposite surfaces of the diamond sensor. The bias voltage provides the necessary electric field across the device that drifts the free charge carriers to be collected in the external circuit as an electric signal.

Ion implantation as described by Prins (1989) and metallization are two commonly utilized methods for the production of ohmic contacts on diamond surfaces. The technique of metallization could be achieved by sputtering (Pan et al., 1993; Schirru et al., 2010) or thermal evaporation (Buttar et al., 1997; Vittone et al., 1999; Whitehead et al., 2001; Galbiati et al., 2001; Ascarelli et al., 2003; Marczewska et al., 2007; Assiamah et al., 2007; Almaviva et al., 2010) in which single or successive metals are used to form the electrical contacts. The metal directly in contact with the diamond surface usually determines the ohmic behaviour of the contact and such a metal should easily form a carbide layer with the diamond surface. Transition metals such as titanium and chromium that form carbides with diamond are commonly used. Gold is usually deposited on the transition metal so as to prevent oxidation due to the inert nature of gold. Annealing typically follows metallization (Ramkumar et al., 2001) in order to allow the transition metal in contact with the diamond surface to form a carbide layer (Vittone et al., 1999) that ensures that the contact exhibits good ohmic behaviour (Whitehead et al., 2001).

The method of metallization using thermal evaporation is frequently utilised, so a diamond radiation detector can be regarded as a sandwich structure consisting of a metal-insulator-metal (MIM) where the diamond (an insulator) is sandwiched between two metal contacts (Kania et al., 1993) as shown in Fig 2.6. The ohmic contacts formed in this way require no n-type or p-type junctions as is required with silicon diodes. Silicon diodes can not be operated with this structure because thermally generated leakage currents are high due to the low band gap of silicon. The high leakage currents in silicon are suppressed by the use of reverse bias junctions. As Fig 2.6 demonstrates, the MIM sandwich structure resembles a parallel-plate capacitor and its mode of operation is similar to that of an ionization chamber based dosimetry system.

2.6 Overview of dosimetry with diamond detectors

Both natural and synthetic diamond crystals have been investigated for dosimetry. The use of natural diamond detectors supplied by PTW (Physikalisch Technische Werkstätten) for dosimetry examined by several researchers (Bampton, 1976; Planskoy, 1980; Heydarian et al., 1993; Vatnitsky and Järvinen, 1993; Laub et al., 1997; Hoban et al., 1994; Rustgi, 1998; Laub et al., 1999; Hugtenburg et al., 2001; Westermark et al., 2002; Björk et al., 2000; Björk et al., 2002; Björk et al., 2004; Barnett et al., 2005; Lambert et al., 2007; Sabino et al., 2012)

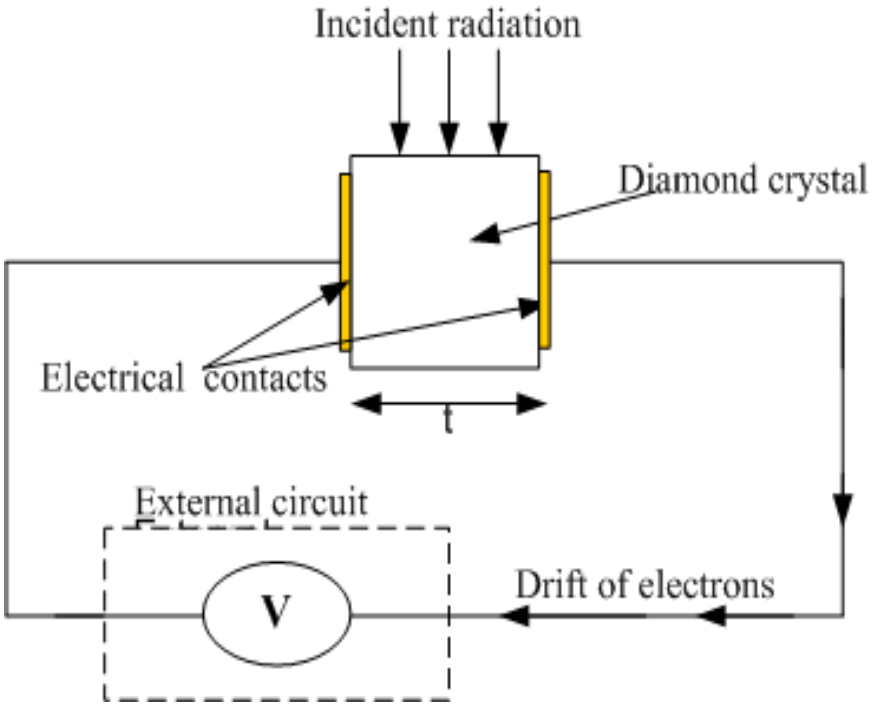

Figure 2.6: Schematic diagram showing a metal-insulator-metal sandwich structure of a diamond radiation detector. The electric field is applied across the two metal contacts.

has been hindered by various drawbacks. The need for daily pre-irradiation due to the presence of uncontrolled amount of impurities and the variation of pre-irradiation dose (between 5 to 15 Gy) (Marsolat et al., 2013); dose rate dependence which varies between devices; high cost and long delivery times due to the scarceness of suitable stones; long selection procedures of diamond stones for suitable detection properties and poor reproducibility between devices are the major limitations of natural diamond detectors (Yacoot et al., 1990; Guerrero et al., 2004; Guerrero et al., 2005; Guerrero et al., 2006; Marsolat et al., 2013). Also, being a natural resource, natural diamond detectors are not readily available (Das, 2009) and hence more difficult to provide[3].

Due to reproducible and optimized growth conditions, synthetic diamond has been considered as a substitute to natural diamond (Burgemeister, 1981; Keddy et al., 1987; Van der Merwe and Keddy, 1999; Benabdesselam et al., 1999; Buttar et al., 2000; Bruzzi et al., 2000; Whitehead et al., 2001; Ramkumar et al., 2001; Fidanzio et al., 2002; Cirrone et al. 2006; Bergonzo et al., 2007; Assiamah et al., 2007; Marczewska et al., 2007; Mavunda et al., 2008; Górka et al, 2008; Tranchant et al., 2008; Gervino et al., 2010; De Angelis et al., 2010; Mohamed Abdel-Rahman et al., 2012) since the impurity levels in synthetic diamond could potentially be controlled to tailor its radiation detection properties (Marsolat et al., 2013). Particularly, synthetic diamond detector has been investigated as: an ionisation chamber in biological environments (Keddy et al., 1987); a TL detector (Nam, 1989); a near-tissue equivalent probe in relative electron dosimetry (Van der Merwe and Keddy, 1999); a probe for low-energy X-ray dose measurements (Assiamah et al., 2007); a dosimeter (Marsolat et al., 2013) and schottky diodes (Ciancaglioni et al., 2012) for small photon beams.

However significant issues which limit dosimetric performance and hence availability of the device remain a challenge and thus require further investigation. These challenges include: rotational inaccuracies due to a difference in geometry between the diamond sensor and its housing; encapsulation of detector material to reduce perturbation and energy dependent effects; daily pre-irradiation and dose rate dependence which are major artefacts; suppression

[3]The so-called PTW natural diamond detector is no longer available in the market. Its waiting period was roughly twelve months and it was approximately seven to eight times more expensive than a Farmer ion chamber (Rustgi, 1998).

of electromagnetic disturbances and other background signals which are sources of noise in radiation measurements; suitable crystal type and size to provide a compromise between sensitivity and spatial resolution for measurements in small fields; practical considerations such as ease of fabrication of the device including convenience of use and compatibility with commercially available electrometer systems; angular response and cable irradiation effects.

2.6.1 The pre-irradiation (priming) and dose rate dependence

Natural as well as synthetic diamond detectors are frequently reported to require priming prior to each measurement (Bampton, 1976; Vatnisky and Jävinen, 1993; Laub et al., 1999; Buttar et al., 2000; Fidanzio et al., 2004; Cirrone et., 2006). Such a procedure is necessary so as to stabilize the sensitivity of a diamond detector before dose measurements (Guerrero et al., 2004; Guerrero et al., 2005). Priming with suitable doses from a few grays to some tens of grays are usually required (Manfredotti, 2005) and a dose of up to 30 Gy has been reported for CVD diamond detectors (Galbiati et al., 2001; Bruzzi et al., 2004). The priming dose depends on defect and impurity levels, which can not be controlled in natural diamond (Marsolat et al., 2013). Nonetheless, Buttar et al. (1997) pointed out the importance to improve the stability of their CVD diamond detectors as they could not stabilize the detectors after pre-irradiating with a dose of 5 Gy. Subsequently, Buttar et al. (2000) improved the performance of their detectors, but noted that additional work is required to understand and eliminate the priming effect.

Diamond detectors are also well known to show dose rate dependence (Planskoy, 1980; Hoban et al., 1994; Laub et al., 1997; Laub et al., 1999; Björk et al., 2000; Hugtenburg et al., 2001; Fidanzio et al., 2004) in accordance with Fowler (1966) theory of induced conductivity in insulators. The change in electrical conductivity, σ of a diamond detector with absorbed dose rate, D_r as expressed below in Eq. (2.1) is known to be influenced by imperfections.

$$\sigma \propto D_r^{\Delta} \qquad (2.1)$$

The dose rate linearity index, Δ can take on a range of values around unity depending on the material characteristics such as the absence or presence of active traps, their capture cross sections and distributions within the detector material. Consequently, the detector may show a sub-linear ($\Delta < 1$), linear ($\Delta = 1$) or supra-linear ($\Delta > 1$) behaviour. Principally, for a pure detector material or when the rate of excitation is so high that the presence of traps become irrelevant, $\Delta = 0.5$; if the carrier lifetime is governed by traps with the same capture cross sections, $0.5<\Delta<1.0$; uniform and quasi-uniform trap distributions over a wide range of

depths in the forbidden gap lead to $\Delta \approx 1$. The value of Δ may exceed unity if traps in the material have differing capture cross sections (Fowler, 1966) or are distributed non-uniformly (Mohamed Abdel-Rahman et al., 2012).

The earlier studies of diamond detectors concluded that the diamond detector fulfils nearly all the dosimetric properties of radiation dosimeters except for the fact that it shows dose rate dependence. As a result, diamond detectors that show a non-linear response with absorbed dose rate require the correction factor Δ for relative dose measurements as noted by Hoban et al. (1994). The factor Δ is an important property of diamond detectors since it determines both the linearity of a given diamond detector and also gives an indication of crystal quality as its value is known to be influenced by the presence or absence of crystal imperfections. Because of its influential role a systematic investigation into the effect of the change in Δ in relative dosimetry and its relationship with various parameters such as bias voltage, beam energy and type including in particular the change of Δ with defect levels, forms part of this thesis. Additionally addressed in this thesis is the issue of daily priming which is an annoying procedure since extra time is required to carry out such step in dosimetry, and it could lead to uncertainty in dose determination if the correct pre-irradiation dose is not given.

2.6.2 Detector geometry and rotational inaccuracy

For accurate dose determination especially for measurements in small fields, the choice of the detector as well as its alignment with the central axis of the radiation beam is relevant. In addition to the major challenges associated with the dosimetry of small fields (section 2.6.3), inaccuracies introduced by slight detector misalignment become significant compared to measurements in large radiation fields due to the presence of steep dose gradients in small fields (Scott et., 2008; Scott et al., 2009; Wuerfel, 2013). As electron dosimetry in particular usually implies the measurements of high dose gradients (Van der Merwe and Keddy, 1999; Lee et al., 2012), detectors with suitable geometries are required to minimize uncertainties. Unlike cylindrical ion chambers which produce significant perturbations in an electron field, the design of parallel-plate chambers minimizes such perturbations (Khan, 2003).

Most diamond detectors often encountered in literature (Heydarian et al., 1993; Van der Merwe et al., 1999; Manfredotti et al., 1998; Hugtenburg et al., 2001; Marczewska et al., 2007; Assiamah et al., 2007; Lansley et al., 2009; Betzel et al., 2010; Tromson et al., 2010; Schirru et al., 2010; De Angelis et al., 2010; Almaviva et al., 2010; Marsolat et al., 2013)

have cylindrical holders that house diamond plates as sensors. The difference in the geometries between the holder (cylindrical) and the diamond sensor (rectangular) is challenging for accurate dosimetry since the configuration is susceptible to rotational uncertainties (that is, the diamond sensor may be misaligned or positioned obliquely relative to the central axis of the beam). Cylindrical designs are also challenging to construct. For instance, in a study reported by Assiamah et al. (2007) describing a synthetic diamond probe for low-energy X-ray dosimetry, the diamond plate was encapsulated in an elongated tubular housing constructed of thermoplastic resin. The shortcomings associated with such a construction are: (i) both precision and time is required in construction and as well in the assembly of the detector; (ii) because of the tubular configuration extra care is required to ensure that the appropriate face is perpendicular to the radiation beam when positioning the detector for accurate dose determination; and (iii) the tubular design complicates the incorporation of materials that are required to remove performance-influencing interferences from environmental sources. As rotational uncertainties translate to dosimetric inaccuracies, this study presents a probe with a suitable geometry that is not susceptible to rotational uncertainties unlike the typical tubular or cylindrical constructions often encountered in literature for diamond detectors.

2.6.3 Small-field dosimetry

Practically the measurement of absorbed dose made with ionization chambers in large radiation fields rely on the assumptions and application of the Bragg-Gray cavity theory where charged particle equilibrium (CPE) exists. CPE exists with respect to a given volume V if each charged particle of a given type and energy leaving V is replaced by an identical particle of the same energy entering V, in terms of expectation values (Attix, 1983). In other words, CPE exists if the energies, number and direction of the charged particles are constant throughout the volume of interest. When the size of the air-filled cavity is smaller than the range of charged particles originating in the medium, the cavity is treated as non-perturbing (Das, 2008). Under such conditions, the absorbed dose in the medium is related to the absorbed dose in the air cavity by the stopping power ratios of medium to air. However, with decreasing field size, neither CPE exists nor the conditions for the cavity theory can be fulfilled as a result of the lateral range of electrons. Consequently, beam models usually designed for measurements in large radiation fields can result in significant uncertainties when used in small fields. For a small field where CPE does not exist, the presence of a

detector can alter the local level of the CPE, adding more perturbations to complicate the problem (Das, 2008).

In general, the dosimetry of small fields is known to be challenging as a result of the non-tissue-equivalence of detectors, their finite size which leads to volume averaging effects and the absence of CPE under small-field conditions (Haryanto et al., 2002; Laub and Wong, 2003; Das, 2009; Lee et al., 2012). The aspects of tissue-equivalence and volume effect are both known to be related to the loss of electronic equilibrium (Haryanto et al., 2002). The equilibrium of secondary electrons breaks down as soon as the distance to the closest field edge is smaller than the travel distance of laterally scattered secondary electrons (Wuerfel, 2013). That is, loss of electronic equilibrium is due to the beam width becoming narrower than the maximum lateral range of secondary electrons. Any detector will average the dose across its sensing volume. But if the dose varies significantly across the volume of the detector, then the effect of averaging can give a different signal compared to the signal that an infinitesimally small detector would measure if placed in the centre of the large detector (Wuerfel, 2013). The so-called volume averaging effect leads to an underestimation of the dose in the centre of a small field when measuring output factors (OFs) (Wuerfel, 2013).

In essence, three parameters are required of detectors for measurements in small fields: high spatial resolution; high sensitivity and tissue-equivalence of the detector material and its housing. High spatial resolution is required to reduce the effects of volume averaging which become significant due to steep dose gradients in small fields. High sensitivity of the detector to radiation is necessary to keep statistical noise and measurement time to an acceptable level (Westermark et al., 2000). High radiation sensitivity also implies that a detector with small sensing volume can be utilised and as result, high spatial resolution can be attained. For some detectors such as air ion chambers, there is a trade-off between sensitivity and spatial resolution. The sensing volume may be small enough to provide good spatial resolution at the expense of signal-to-noise ratio (SNR) or it may be large enough to provide a high SNR but at the expense of spatial resolution. As diamond is a wide bandgap material compared to silicon, the SNR of a diamond detector is expected to be better than that of a diode detector at room temperature since the noise level arising from leakage currents is relatively low.

As pointed out in chapter one (section 1.5) the perturbation correction factor, P_{pert} is required if the detector perturbs the relationship between the absorbed dose to medium and the

response of the detector. The perturbation factor can be defined as the deviation of the perfect Bragg-Gray/Spencer-Attix theory (Björk et al., 2000). However, to assess the absorbed dose to tissue with the highest possible accuracy the detector and its housing should be similar in atomic composition to the medium. Such a detector would not extensively perturb the electron fluence produced in the medium and its response to radiation would be proportional to the absorbed dose to tissue over a broad energy range. Local changes in electronic equilibrium could also result due to the presence of non-tissue equivalent dosimeters.

Consequently, the tissue-equivalence of a detector and its encapsulation is necessary to minimise the loss of CPE and perturbation effects. Perturbation effects have been shown to have a significant influence in field sizes less than 1 cm in width for solid state detectors such as diodes (Somigliana et al., 1999; Westermark et al., 2000; Haryanto et al., 2002; Laub and Wong, 2003; Scott et al., 2012). Beam quality usually changes under small-field conditions as a result of the variation of the contribution of scattered photons. Since high atomic number materials are sensitive to low-energy photons, tissue-equivalent detectors are required for measurements in small fields so that their response should not vary with beam energy.

Accurately measured small-field OFs are relevant beam data which are used to determine monitor units for dose delivery. As a result, a number of studies have compared OFs measured with different commercially available detectors such as ion chambers, silicon diodes and PTW natural diamond in small fields aimed at selecting a suitable detector (Westermark et al., 2000; Haryanto et al., 2002; Laub and Wong, 2003; Björk et al., 2004; Barnett et al., 2005; Das et al., 2008). Significant differences in the OFs were obtained with the different detectors. The results of most of the studies however indicated that the diamond detector is the most appropriate small-field detector due to its excellent dosimetric properties such as its small physical size (high spatial resolution) and near-tissue equivalence (Haryanto et al., 2002; Laub and Wong, 2003; Björk et al., 2004). The use of small-volume ion chambers is limited to a field size of 2 x 2 cm^2. OFs obtained with field sizes below this limit are underestimated due to an increase in lateral electronic disequilibrium and the effects of volume averaging caused by the relatively large size of the air cavity (Haryanto et al., 2002; Laub and Wong, 2003). For silicon diodes, they have been shown to overestimate the OF in fields $\leq$ 1 x 1 cm^2 due to the non-tissue equivalence of silicon (Haryanto et al., 2002).

In spite of the limitations of natural diamond detectors, only a few studies (Almaviva et al., 2010; Ciacaglioni et al., 2012; Marsolat et al., 2013) have evaluated the performance of relatively small-sized synthetic diamond detectors (single crystal CVD diamonds) under small-field conditions. The sensitivity values of these devices were however not reported. In addition, the relationship between diamond detector-size and field size to provide a guide for crystal size selection for measurements in small fields has not been investigated.

2.6.4 Other challenges which limit the performances of diamond detectors

It is known that dark currents and their instabilitys are a limiting factor for efficient collection of charge carriers since they are a detrimental source of noise in radiation measurements and can limit the size of the applied electric field (Kania et al., 1993; Fidanzio et al., 2002; Fidanzio et al., 2004). Electromagnetic disturbance from the linac environment also acts as a source of noise (Wuerfel, 2013). Tartoni et al. (2009) reported placing their diamond detector in an earthed metal box in order to reduce electrostatic noise that might be picked up. Although in principle diamond is characterised by low leakage currents at room temperatures as it is a wide bandgap material, it is also a high impedance material and high impedance devices tend to be more susceptible to the presence of noise. Dark current values of up to 4 nA and 12 nA have been measured by Galbiati et al. (2001) for a CVD diamond detector before and after irradiation, respectively. With such a large variation of the leakage current between irradiations, it is usually required to wait for several minutes for the dark current to drop to its initial value before proceeding with measurements. It is therefore indispensable to optimize the design of diamond detectors so as to suppress noisy backgrounds.

To reduce perturbation effects, it is necessary to have detectors with small physical sizes. This requirement is essential for measurements in small radiation fields but it poses a problem for the dosimetry of large fields due to cable irradiation effects. For instance, for the evaluation of the angular dependence of small-sized diamond detectors, a small radiation field of size $\leq 4 \times 4$ cm^2 is usually chosen to avoid cable irradiation (Westermark et al., 2000; Ciacaglioni et al., 2012). Other contributions to the angular response of detectors could arise from encapsulating materials including electrodes and interface phenomena (Rikner, 1985; Heydarian et al., 1993). It is known for CVD diamond detectors that the magnitude of the interface effects (i.e., the distortion of the mean absorbed dose in the sensitive volume of the detector) due to metallic contacts strongly depends on the thickness of the metallised diamond, the atomic number of the metal contacts and the energy of radiation; with the effect

lessening with increasing diamond thickness and radiation energy, but increases with increase in metal thickness and their atomic number (Górka, 2008).

The literature survey thus indicates that the dosimetric performance of an ionising radiation detector such as a diamond detector strongly depends on its design and inherent properties such as dose rate dependence. Furthermore, data for the use of synthetic diamond detectors in small-fields especially for fields below 1 x 1 cm^2 are relatively scarce. In this thesis, an improved design of a diamond probe is presented which addresses various challenges for measurements in large and small radiation fields. Additionally, the relationship between crystal size and field size is investigated with the aim of selecting suitable crystals and crystal size for measurements under small and very small-field conditions. A comparison of the sensitivity values of a commercially available small-field detector and the synthetic diamond probe is conducted.

References

Almaviva, S., Ciacaglioni, I., Consorti, R., De Notaristefani, F., Manfredotti, C., Marco Marinelli, Milani, E., Petrucci, A., Prestopino, G., Verona, C., Verona-Rinati, G. 2010. Synthetic single crystal diamond dosimeters for conformal radiation therapy application. *Diamond Relat. Mater.* **19**, 217.

Ascarelli, P., Cappelli, E., Trucchi, D.M., Conte, G., 2003. CVD diamond dosimetric response evaluated by X-ray absorbers method. *Diamond Relat. Mater.* **12**, 691.

Assiamah, M., Nam, T.L., Keddy, R.J., 2007. A synthetic diamond probe for low-energy X-ray dose measurements. *Appl. Radiat. Isot.* **65**, 545.

Attix, F.H., 1983. Energy imparted, energy transferred and net energy transferred. *Phys. Med. Biol*. **28**, 1385.

Balmer, R.S., Brandon, J.R., Clewes, S.L., Dhillon, H.K., Dodson, J.M., Friel, I., Inglis, P.N., Madgwick, T.D., Markham, M.L., Mollart, T.P., Perkins, N., Scarsbrrok, G.A., Twitchen, D.J., Whitehead, A.J., Wilman, J.J, Woollard, S.M., 2009. Chemical vapour deposition synthetic diamond: materials, technology and applications *J. Phys.: condens. Matter* **21**, 364221.

Bampton, F.K., 1976. A medical application for radiosensitive diamonds. *Ind. Diamond Rev.* **36,** 55.

Barnett, E., MacKenzie, M., Fallone, B., G 2005. IMRT point dose measurements with a diamond detector. *Radiol. Oncol.* **39**, 71.

Benabdesselam, M., Iacconi, P., Briand, D., Lapraz, D., Butler, J. E. 1999. Selected thermo-luminescent properties of CVD diamond film. *Radiation Protection Dosimetry*, **84**, 257.

Bergonzo, P., Tromson, D., Descamps, C., Hamrita, H., Mer, C., Tranchant, N., Nesladek, M., 2007. Improving diamond detectors: A device case *Diamond Relat. Mater.* **16**, 1038.

Betzel, G.T., Lansley, S.P., Baluti, F., Reinisch, L., Meyer, J. 2010. Operating parameters of CVD diamond detectors for radiation dosimetry. *Nucl. Instrum. Methods Phys. Res*. A **614**, 130.

Björk, P., Knöös, T., Nilsson, P., 2000. Comparative dosimetry of diode and diamond detectors in electron beams for intraoperative radiation therapy. *Med. Phys.* **27,** 2580.

Björk, P., Nilsson, P., Knöös, T., 2002. Dosimetry characteristics of degraded electron beams investigated by Monte Carlo calculations in a setup for intraoperative radiation therapy. *Phys*. *Med. Biol*. **47**, 239.

Björk, P., Knöös, T., Nilsson, P., 2004. Measurements of output factors with different detector types and Monte Carlo calculations of stopping-power ratios for degraded electron

beams. *Phys. Med. Biol.* **49,** 4493.

Breeding, C.M., Shigley, J.E., 2009. The “Type” classification system of diamonds and its importance in Gemology. *Gems & Gemology*, Summer 2009. 96-111.

Bruzzi, M., Bucciolini, M., Cirrone, G.A.P., Cuttone, G., Mazzocchi, S., Pirollo, S., Sciortino, S., 2000. Characterisation of CVD diamond dosimeters in on-line configuration. *Nucl. Instrum. Methods Phys. Res*. A **454**, 142.

Bruzzi, M., Bucciolini, M., Casati, M., DeAngelis, C., Lagomarsino, S., Løvik, I., Onori, S., Sciortino, S., 2004. CVD diamond particle detectors used as on-line dosimeters in clinical radiotherapy. *Nucl. Instrum. Methods Phys. Res*. A **518**, 421.

Burgemeister, E.B., 1981. Dosimetry with a diamond operating as a resistor. *Phys. Med. Biol.* **26**, 269.

Buttar, C.M., Conwayb, J., Meyfarth, R., Scarsbrook, G., Sellin, P.J., Whitehead, A., 1997. CVD diamond detectors as dosimeters for radiotherapy. *Nucl. Instrum. Methods Phys. Res*. A **392**, 281.

Buttar, C.M., Airey, R., Conway, J., Hill, G., Ramkumar, S., Scarsbrook, G., Sussmann, R.S., Walker, S., Whitehead, A. 2000. A study of radiotherapy dosimeters based on diamond grown by chemical vapour deposition. *Diamond Relat. Mater*. **9**, 965.

Calzaferri, G., Rytz, R., 1996. The Band Structure of Diamond. *J. Phys. Chem.* **100**, 11122.

Ciancaglioni, I., Marco Marinelli, Milano, E., Prestopino, G., Verona, C., Verona-Rinati, G., Consorti, R., Petrucci, A., De Notaristefani, F., 2012. Dosimetric characterization of a synthetic single crystal diamond detector in clinical radiation therapy small photon beams. *Med. Phys.* **39**, 4493.

Cirrone, G.A.P., Cuttone, G., Lo Nigro, S., Mongelli, V., Raffaele, L., Sabini, M.G., 2006. Dosimetric characterization of CVD diamonds in photon, electron and proton beams. *Nucl. Phys. B (Proc. Suppl.)* **150**, 330.

Das, I.J., Ding, G.X., Ahnesjö, A., 2008. Small fields: Nonequilibrium radiation dosimetry. *Med. Phys.* **35**, 206.

Das I.J., Diamond detector In: Rogers, D.W.O., Cyglar JE, Clinical Dosimetry Measurements in Radiotherapy. Madison, WI: *Medical Physics Publishing*, 2009. pp. 891-912.

De Angelis, C., Bucciolini, M., Viscomi, D., Marczewska, B., Onori, S., 2010. Characterization of a HPHT diamond detector for clinical applications. *Nucl. Instrum. Methods Phys. Res*. A **612**, 576.

Fowler, J.F., 1966. Solid state electrical conductivity dosimeters. Radiation Dosimetry. vol. II. New York: Academic. pp 291.

Galbiati, A., Breese, M.B.H., Knights, A.P., Sealy, B., Sellin, P.J., 2001. Characterisation of a coplanar CVD diamond radiation detector. *Nucl. Instrum. Methods Phys. Res*. A **466**, 52.

Gervino, G., Marino, C., Silvestri, F., Lavagno, A., Truc, F., 2010. Dosimetry with diamond detectors. *Nucl. Instrum. Methods Phys. Res*. A **617**, 230.

Górka, B., Nilsson, B., Svensson, R., Brahme, A., Ascarelli, P., Trucchi, D.M., Conte, G., Kalish, R., 2008. Design and characterization of a tissue-equivalent CVD-diamond detector for clinical dosimetry in high-energy photon beams. *Physica Medica,* **24**, 159.

Gracio, J.J., Fan, Q.H., Madaleno, J.C., 2010. Diamond growth by chemical vapour deposition. *J. Phys. D: Appl. Phys.* **43**, 374017.

Guerrero, M.J., Tromson, D., Rebisz, M., Mer, C., Bazin, B., Bergonzo, P., 2004. Requirements for synthetic diamond devices for radiotherapy dosimetry applications *Diamond Relat. Mater.* **13**, 2046.

Guerrero, M.J., Tromson, D., Bergonzo, P., Barrett, R., 2005. Investigation of defects in CVD diamond: Influence for radiotherapy applications. *Nucl. Instrum. Methods Phys.Res*. A **552**, 105.

Guerrero, M.J., Tromson, D., Descamps, C., Bergonzo, P., 2006. Recent improvements on the use of CVD diamond ionisation chambers for radiotherapy applications. *Diamond Relat. Mater.* **15**, 811.

Haryanto, F., Fippel, M., Laub, W., Dohm, O., Nüsslin, F., 2002. Investigation of photon beam output factors for conformal radiation therapy—Monte Carlo simulations and measurements *Phys. Med. Biol.* **47**, N133.

Heydarian, M., Hoban, P.W., Beckham, W.A., Borchardt, I.M, Beddoe, A.B., 1993. Evaluation of a PTW diamond detector for electron beam measurements. *Phys. Med. Biol*. **38**, 1035.

Hoban, P.W., Heydarian, M., Beckham, W.A., Beddoe, A.H., 1994. Dose rate dependence of a PTW diamond detector in the dosimetry of a 6 MV photon beam. *Phys. Med. Biol*. **39**, 1219.

Hugtenburg, R.P., Kristen, J., Graham, J.C., Alun H.B., 2001. Application of diamond detectors to the dosimetry of 45 and 100 kVp therapy beams: comparison with a parallel-plate ionization chamber and Monte Carlo. *Phys. Med. Biol.* **46**, 2489.

Kalish, R., 2007. Diamond as a unique high-tech electronic material: difficulties and prospects. *J. Phys. D: Appl. Phys.* **40,** 6467.

Kania, D.R., Landstrass, M.I., Plano, M.A., 1993. Diamond radiation detectors. *Diamond Relat. Mater.* **2**, 1012.

Keddy, R.J., Nam, T.L., Burns, R.C., 1987. Synthetic diamonds as ionisation chamber radiation detectors in biological environments. *Phys. Med. Biol.*, **32**, 751.

Khan, F.M. The Physics of Radiation Therapy, 3rd ed. Philadelpia: Lippincott & Wilkins, 2003.

Lambert, J., Nakano, T., Law, S., Elsey, J., McKenzie, D.R., Suchowerska, N., 2007. *In vivo* dosimeters for HDR brachytherapy: A comparison of a diamond detector, MOSFET, TLD, and scintillation detector. *Med. Phys.* **34**, 1759.

Lansley, S.P., Betzel, G.T., Meyer, J., Baluti, F., Reinisch, L., Meyer, J., 2009. Investigation of the suitability of commercially available CVD diamond for megavoltage X-raydosimetry. *Nucl. Instrum. Methods Phys. Res.* A **607**, 659.

Laub, W.U., Wong, T., 2003. The volume effect of detectors in the dosimetry of small fields used in IMRT. *Med. Phys.* **30**, 341.

Laub, W.U., Kaulich, T.W., Nusslin, F., 1997. Energy and dose rate dependence of a diamond detector in the dosimetry of 4–25 MV photon beams. *Phys. Med. Biol.* **24**, 535.

Laub, W.U., Kaulich, T.W., Nusslin, F., 1999. A diamond detector in the dosimetry of high-energy electron and photon beams . *Phys. Med. Biol.* **44**, 2183.

Lee, S. H., Kim, J., Nam, Y. S., Cho SamJu, Kwon, S., Lee, S., Shim, J.B., Kim, C.Y., Min, C.K., Cho, K.H., Huh, HyunDo, 2012. Analysis of Output Factors with Various Detectors in Small-field Electron-beam Radiotherapy. *Journal of the Korean Physical Society,* **60**, 875.

Mainwood, A., 2000. Recent developments of diamond detectors for particles and UV radiation. *Semicond. Sci. Technol.* **15**, R55.

Manfredotti, C., Apostolo, G., Fizzotti, F., Lo Giudice, A., Morando, M., Pignolo, R., Polesselo, P., Truccato, M., Vittone, E., Nastasi, U., 1998. CVD diamond tips as X-ray detectors. *Diamond Relat. Mater.* **7**, 523.

Manfredotti, C., 2005. CVD diamond detectors for nuclear and dosimetric applications. *Diamond Relat. Mater.* **14**, 531.

Marczewska, B., Kupriyanov, I., Pal'Yanov, Yu., Nowak, T., Olko, P., Rębisz, M., Waligórski, M.P.R., 2007. A study of radiation dosimeters based on synthetic HPHT diamond. *Diamond Relat. Mater.* **16**, 191.

Marsolat1, F., Tromson, D., Tranchant, N., Pomorski, M., Le Roy, M., Donois, M., Moignau, F., Ostrowsky, A., De Carlan, L., Bassinet, C., Huet, C., Derreumaux, S., Chea, M., Cristina, K., Boisserie, G., Bergonzo, P., 2013. A new single crystal diamond dosimeter for small beam: comparison with different commercial active detectors. *Phys. Med. Biol.* **58**, 7647.

Mavunda, R.D., Zakari, Y.I., Nam, T.L., Keddy, R.J., 2008. The presence of defects and their influence on the performance of CVD diamond as an α-particle radiation sensing element. *Appl. Radiat. Isot.* **66,** 1128**.**

Mohamed Abdel-Rahman, A.E., Lohstroh, A., Jayawardena, I., Henley, S.J., 2012. The X-ray detection performance of polycrystalline CVD diamond with pulsed laser deposited carbon electrodes. *Diamond Relat. Mater.* **22**, 70.

Nam, T.L., 1989. Nuclear radiation detection properties of diamond. *PhD Thesis, University of the Witwatersrand, Johannesburg*.

Pan, L. S., Han, S., Kania, D. R., 1993. Electrical properties of high quality diamond films. *Diamond Relat. Mater.* **2**, 820.

Planskoy, B., 1980. Evaluation of diamond radiation dosemeters. *Phys. Med. Biol.* **25**, 519.

Prins, J.F., 1989. Preparation of ohmic contacts to semiconducting diamond. *J. Phys. D: Appl. Phys.* **22**, 1562.

Ramkumar, S., Buttar, C.M., Conway, J., Whitehead, A.J., Sussman, R.S., Hill, G., Walker, S., 2001. An assessment of radiotherapy dosimeters based on CVD grown diamond. Nucl. Instrum. Methods Phys. Res. A **460**, 401.

Rikner, G., 1985. Characteristics of a p-Si detector in high energy electron fields. *Acta Radiol. Oncology* **24**, 71.

Rustgi, S.R., 1998. Application of a diamond detector to brachytherapy dosimetry. *Phys. Med. Biol.* **43,** 2085.

Sabino, T., Rodrigues, L.N., Furnari, L., Watanabe, E.Y., Menegussi, G., 2012. *Radiol. Bras*. **45**, 35.

Schirru, F., Kisielewicz, K., Nowak, T., Marczewska, B., 2010. Single Crystal Diamond Detector for Radiotherapy. J. Phys. D: Appl. Phys. **43**, 265101.

Scott, A.J.D., Nahum, A.E., Fenwick, J.D., 2008. Using a Monte Carlo model to predict dosimetric properties of small radiotherapy photon fields. *Med. Phys.* **35,** 4671.

Scott, A.J.D., Nahum, A.E., Fenwick, J.D., 2009. Monte Carlo modeling of small photon fields: Quantifying the impact of focal spot size on source occlusion and output factors, and exploring miniphantom design for small-field measurements. *Med. Phys.* **36,** 3132.

Scott, A.J.D., Kumar, S., Nahum, A.E., Fenwick, J.D., 2012. Characterizing the influence of detector density on dosimeter response in non-equilibrium small photon fields. *Phys. Med. Biol.* **57**, 4461.

Somigliana, A., Cattaneo, G.M., Fiorino, C., Borelli, S., del Vecchio, A., Zonca, G., Pignoli, E., Loi, G., Calandrino, R., Marchesini, R., 1999. Dosimetry of Gamma Knife and linac-

based radiosurgery using radiochromic and diode detectors. *Phys. Med. Biol.* **44**, 887.

Tartoni, N., Angelone, M., Pillon, M., Almaviva, S., Marinelli, M., Milani, E., Prestopino, G., Verona, C., Rinati, G.V., Roberts, M.A., 2009. X-Ray Detection by Using CVD Single Crystal Diamond Detector. *IEEE Transactions on Nuclear Science*, **56**, 849.

Taylor, W.R., Jacques, A.L., Ridd, M., 1990. Nitrogen-defect aggregation characteristics of some Australasian diamonds: Time-temperature constraints on the source regions of pipe and alluvial diamonds. *American mineralogist*, **75**, 1290.

Tranchant, N., Tromson, D., Descamps, C., Isambert, A., Hamrita, H., Bergonzo, P., Nesladek, M., 2008. High mobility single crystal diamond detectors for dosimetry: Application to radiotherapy. *Diamond Relat. Mater.* **17**, 1297.

Tromson, D., Rebisz-Pomorska, M., Tranchant, N., Isambert, A., Moignau, F., Moussier, A., Marczewska, B., Bergonzo, P., 2010. Single crystal CVD diamond detector for high resolution dose measurement for IMRT and novel radiation therapy needs. *Diamond Relat. Mater.* **19**, 1012.

Van der Merwe, D.G., Keddy, R.J., 1999. Relative electron dosimetry using a synthetic diamond probe. *Radiat. Phys. Chem.* **54**, 325.

Vatnisky, S., Järvinen, H., 1993. Application of a natural diamond detector for the measurement of relative dose distributions in radiotherapy. *Phys. Med. Biol.* **38**, 173.

Vittone, E., Fizzotti, F., Lo Giudice, A., Polesello, P., Manfredotti, C., 1999. Room temperature CVD diamond X-ray and charged particle microdetectors. *Nucl. Instrum. Methods Phys. Res*. A **428**, 118.

Walker, J. 1979. Optical absorption and luminescence in diamond. *Rep. Prog. Phys.* **42**, 1606.

Westermark, M., Arndt, J., Nilsson, B., Brahme, A., 2000. Comparative dosimetry in narrow high-energy photon beams. *Phys. Med. Biol.* **45**, 685.

Whitehead, A.J., Airey, R., Buttar, C.M., Conway, J., Hill, G., Ramkumar, S., Scarsbrook, G.A., Sussmann, R.S., Walker, S., 2001. CVD diamond for medical dosimetry applications. *Nucl. Instrum. Methods Phys. Res.* A **460**, 20.

Woods, G.S., 1986. Platelets and the infrared absorption of type Ia diamonds. *Proc. R. Soc. Lond.* A **407**, 219.

Wuerfel, J.U., 2013. Dose measurements in small fields. *Med. Phys. Int. J.* **1**, 82.

Yacoot, A., Moore, M., Makepeace, A., 1990. X-ray studies of synthetic radiation-counting diamonds. *Phys. Med. Biol.*, **35**, 1409.

Ziman, J.M., 1972. Principles of the Theory of Solids, 2nd Edition, Cambridge.

CHAPTER THREE

CHARACTERIZATION TECHNIQUES AND PRESENTATION OF PROTOTYPE DESIGN OF MULTI-PURPOSE SYNTHETIC DIAMOND PROBE

3.1 Introduction

The electronic properties of diamond are known to be governed by defects, dopants, grain boundaries and surface defects (Nebel, 2003). For instance, in the field of diamond radiation detectors, it is known that the priming dose and the dose rate linearity index Δ in Fowler's theory (Fowler, 1966) is governed by impurity or trapping levels. While a certain concentration of impurities is required for the signal to increase linearly with dose rate, excess impurities will cause the diamond to be insensitive to radiation and to suffer polarization effects (Hoban et al., 1994; Laub et al., 1999). However, pertinent defect types which could influence Δ are yet to be identified and isolated. To date and to the best of our knowledge, only the study by Marczewska et al. (2007) has highlighted that Δ (evaluated under ^{60}Co radiation) varies with nitrogen concentration but it is not clear in their study which type of nitrogen impurity is causing the variation.

This chapter presents the synthetic diamond crystals under investigation in this thesis and also briefly describes the various techniques (Raman spectroscopy, electron spin resonance (ESR), Fourier transform infrared (FTIR) absorption spectroscopy, thermo-luminescence (TL) and electrical) that were used to characterize the electrical quality and various defect types present within each of the samples. These techniques were chosen because of their valuable and non-destructive properties and wide use. A prototype design and construction of an optimized (i.t.o. environmental and positional influences, encapsulation and contact materials) multi-purpose synthetic diamond probe for dosimetry applications is also presented including various dosimetric parameters or techniques (section 3.10) that were used to evaluate the performance of the probe and the various diamond sensors.

3.2 Synthetic diamond crystals used for this study

Initially nine commercially available synthetic diamond crystals of various types and classes with sizes ranging between 5x5 mm^2 and 10x10 mm^2 and thickness of either 0.5 or 1.0 mm were investigated. These included one HPHT single crystal (HPHT1) and eight polycrystalline CVD diamond crystals of detector grade (DG) and optical grade (OG) qualities (Table 3.1). Shown in Fig. 3.1 is a CVD diamond plate. Subsequent to the results of dosimetric characterizations of the diamond crystals, a small-size HPHT diamond (HPHT2) of dimensions ≈ 3x3x1 mm^3 was deliberately selected for evaluation of its potential application in small radiation fields. In chapters 4 and 7, HPHT1 is labelled simply as HPHT, and in chapter 8, HPHT1 and HPHT2 are labelled as HP1 and HP2, respectively.

3.3 Raman spectroscopy

Raman spectroscopy is a technique that analyzes the inelastic scattering of radiation from atoms of a material that has been illuminated by monochromatic light from a laser. A small fraction of the photons interact with the optic modes of lattice phonons in the material under test and are scattered inelastically. The scattered photons have a frequency that is shifted from the incident photons by the frequency of the vibrational mode which is characteristic of the material (Erasmus et al., 2011). Therefore, inelastic or Raman scattering is the result of the small probability of an incoming light beam interacting and exchanging energy with the sample material.

Raman spectroscopy is a non-destructive tool that has been widely used to characterize the crystal structure of diamonds (Kirillov and Reynolds, 1994; Catledge et al., 1996; Bergman and Nemanich, 1995; Faggio et al., 1999; Prawer and Nemanich, 2004; Pickard et al., 1998; Ascarelli et al., 1985; Knight and White, 1989; Blum et al., 1998 ; Fish et al., 1999; Assiamah et al., 2007; Mavunda et al., 2008; Gracio et al., 2010; Erasmus et al., 2011; Lansley et al., 2009 ; Tranchant et al., 2010). As observed in pure natural diamonds, a single sharp line at 1332 cm^{-1} having a full-width-at-half-maximum (FWHM) of about 2 cm^{-1} (Pickard et al., 1998; Faggio et., 1999) is a commonly accepted fingerprint of the diamond structure (sp^3 phase) (Ascarelli et al., 1985; Knight and White, 1989). The line-width relates to the lifetime of the phonons from which the laser light is scattered (Pickard et al., 1998). In synthetic diamond, the line can be shifted due to internal stress and the width is typically much broader than that observed in natural diamond due to crystal defects or non-homogeneous distribution of stress (Pickard et al., 1998; Faggio et al., 1999; Fish et al., 1999). Furthermore, a feature frequently observed in the Raman spectrum of synthetic diamond is a shoulder and broader

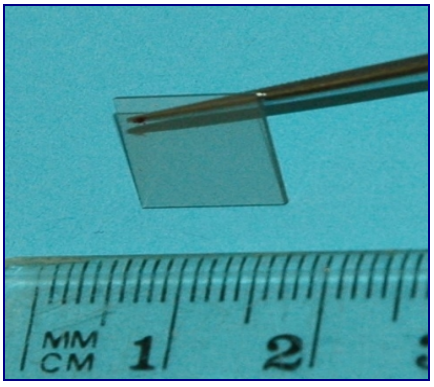

Figure 3.1: A CVD diamond plate

peak around 1335 cm^{-1} and 1500 cm^{-1}, respectively due to the presence of sp^2-bonded carbon (Gracio et al., 2010; Prawer and Nemanich, 2004). Three quality factors are therefore commonly introduced for the quantitative comparison of different diamond crystals (Faggio et al., 1999; Prawer and Nemanich, 2004): the ratio of the non-diamond (sp^2) to the diamond (sp^3) component for phase purity, the Raman FWHM of the diamond Raman peak for crystalline quality and the shift of the peak position for internal stress state.

Seeing that the Raman spectrum of diamond contains a wealth of information, this study utilizes the technique to characterize the phase and crystalline (defect levels) qualities of the diamond crystals under investigation. The Raman spectra were acquired at room temperature using a Jobin-Yvon T64000 Raman spectrometer (Fig. 3.2) operated in a single spectrograph mode with a grating that consists of 1800 grooves/mm and a charge coupled detector (CCD) which collected backscattered Raman signal. The spectra were excited with the 514.5 nm line of an Ar^+ laser and the 20x objective of an Olympus microscope was used to focus the laser beam (spot size 5 µm) with a sampling depth that varies between 40 and 50 µm. In order to improve the statistical significance of the data, the Raman spectra were mapped at twenty different and uniformly spaced spots on the surface of each sample. For each spot, the data

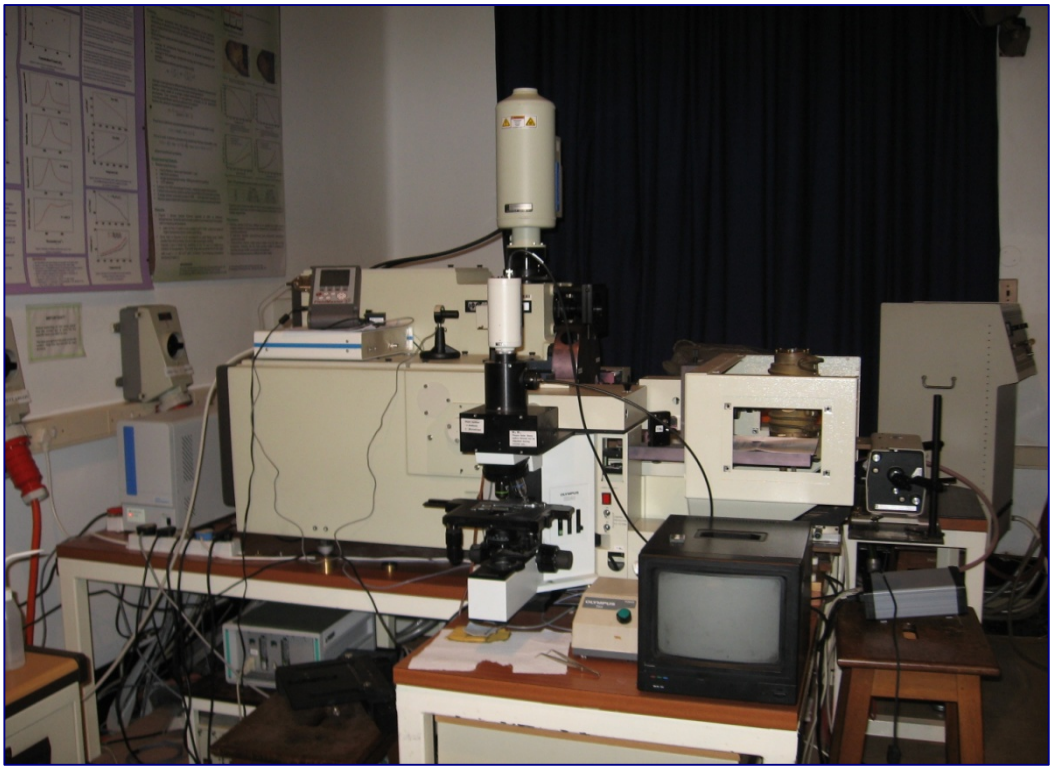

Figure 3.2: Raman spectroscopy unit at the University of the Witwatersrand

were fitted with a combined Gaussian-Lorentzian function in order to extract the diamond peak position and width values. A Lorentzian profile with broadening is caused by a decrease in phonon lifetime due to scattering by lattice defects whereas a Gaussian profile results due to lattice strain caused by defects (Kirillov and Reynolds, 1994). A software package, ORIGIN 8.0 was used for both baseline insertion and background subtraction.

For every single sample under study, only the characteristic diamond Raman peak at approximately 1332.8 cm^{-1} (Fig. 3.3) was observed over a linear background with no observable peaks around 1335 cm^{-1} and 1500 cm^{-1} which is therefore strong evidence that the crystals are pure diamonds (Prawer and Nemanich, 2004; Lansley et al., 2009). Presented in Table 3.1 are values of the Raman FWHM determined from the spectra which ranged between 2.27 and 2.60 cm^{-1} after correction for instrumental contribution. As mentioned earlier, while the diamond Raman peak position can be shifted due to residual stress, the broadening of the line-width is known to be influenced by crystal defects or non-uniform distribution of stress. The results of this study (presented in chapter seven) nonetheless suggest that the broadening in the examined crystals could be mainly linked to defect levels. Realising that the Raman FWHM is a measure of defect concentration (such as point defects, inclusions, grain boundaries) within the crystal lattice, the HPHT diamond having the smallest width of 2.27 cm^{-1} is therefore the least defective crystal whereas DGA1 having the broadest width (2.60 cm^{-1}) is the most defective crystal.

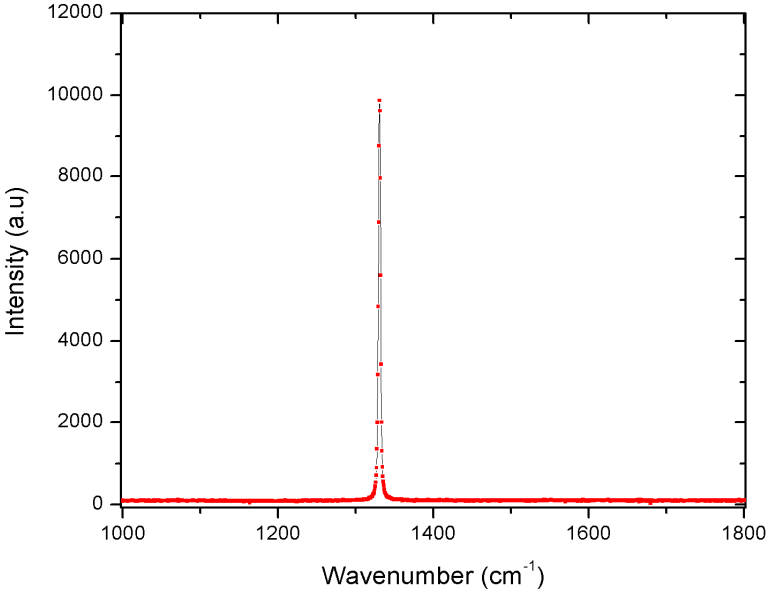

Figure 3.3: Raman spectrum of a HPHT diamond crystal showing the diamond peak at 1332 cm^{-1}

Table 3.1: Synthetic diamond crystals and their parameters

Sample	Dimensions (mm^3)	Raman FWHM (cm^{-1})	ESR N_s level		FTIR absorption area under peak (a.u) [C-H]	[A/B]	[N3]	[A]	TL response (a.u)	J_o values at 1.0 kV/cm (A/cm^2)
HPHT1	8.0x6.4x1.0	2.27±0.04	130		4	3	34	--	2.2	2.0×10^{-11}
OGA1	5.0x5.0x1.0	2.56 ±0.09	43		20	26	60	--	13.8	2.8×10^{-10}
OGA2		2.42±0.09	71	±2 ppm	14	31	55	--	11.4	2.8×10^{-10}
DGA1	5.0x5.0x1.0	2.60±0.13	3.5		65	50	143	2	45.0	1.4×10^{-9}
DGA2		2.55±0.09	5.0		36	22	78	1	19.1	5.6×10^{-10}
DGA	10.0x10.0x0.5	2.34±0.08	20		12	27	19	--	0.74	1.4×10^{-10}
DGB1		2.37±0.11	10	±2 ppb	14	37	39	--	0.82	7.0×10^{-11}
OGA	10.0x10.0x1.0	2.42±0.11	50		6	11	7	1	1.24	2.0×10^{-10}
OGD		2.46±0.25	46		15	12	19	3	1.76	2.5×10^{-10}

3.4 Electron paramagnetic resonance (EPR) or ESR

As a commonly observed impurity in diamond, nitrogen (N) is known to influence its radiation detection properties. Whereas N is difficult to eliminate during the growth process of HPHT diamonds and it is incorporated in different amounts in different growth sectors, its presence in natural diamonds indicates that it is usually involved during their growth (Balmer et al., 2009). For the case of the CVD process, addition of ppm levels of N is known to modify the morphology and texture of polycrystalline films and subsequently weaken grain boundaries (Balmer et al., 2009). Nam et al. (1991) reported that single substitutional N (N_s) is an impurity type accountable for the performance characteristics of diamond radiation detectors. High concentration of N_s lower trap levels when compared to crystals synthesized with lower N_s levels. In addition, diamonds with high N_s levels have a high recombination efficiency which compromises their response (Nam, 1989).

ESR is a powerful and non-destructive technique for the characterisation of point defects in solids (Walker, 1979) and has been successfully used by Loubser and van Wyk (1981) and Fallon (1989) for the determination of the concentration of N_s ($[N_s]$) in diamond. N_s could be easily identified by ESR as ^{14}N, the most common isotope of N, is virtually the only isotope with unit nuclear spin, and because N is a common impurity in diamond (Walker, 1979). The ESR method utilizes the paramagnetic nature of N in a diamond lattice. When the N atom substitutes for a C atom in the diamond lattice, the paramagnetic electron is sited in an antibonding orbital between the N and one of the nearest-neighbour C atoms (Walker, 1979; Fallon, 1989). That is, upon occupying the substitutional site in the diamond lattice, four of the five valence electrons of the N atom bonds tetrahedrally with the four neighboring C atoms. The unpaired electron from the N atom then forms a C-N anti-bonding orbital that is uniformly distributed over the four bonds causing the paramagnetic nature of N_s.

ESR measurements were conducted with a Bruker ESP300E ESP spectrometer unit (Fig. 3.4) operated at a frequency of 9 GHz in similar procedures as reported by Assiamah (2004) and Mavunda (2008) by placing each diamond sample in turn in a magnetic field and using microwave radiation to excite electrons to higher energy levels. The excited electrons absorbed the microwaves when they are at the appropriate wavelength or frequency. The ESR spectrum is a plot of the derivative of the absorbed signal as a function of magnetic field intensity. The measured ESR signal relies on the interaction between the spin angular momentum of a lone electron and an external magnetic field. The degeneracy of the spin

states of the lone electron which is characterized by the quantum number $m_s = \pm ½$ is lifted in the magnetic field and transitions between the spin levels are induced by radiation of appropriate wavelength.

In a magnetic field, the electron spin levels are separated by an amount, which depends on the magnitude of the field. When equilibrium is established there is a difference in the populations between the two levels. When the magnetic field is altered so that the energy difference between the two spin levels equals the energy of the microwaves, transitions are induced between the two levels giving rise to an ESR signal. The observation of the ESR signal relies on maintaining the population difference between the spin levels. This in turn depends on the relaxation times. For high N_s levels, the relaxation times are short and the ESR signal is easily detected. When the N_s levels are low, the relaxation times become long and the population difference between the spin levels becomes smaller making it a challenge to detect the ESR signal.

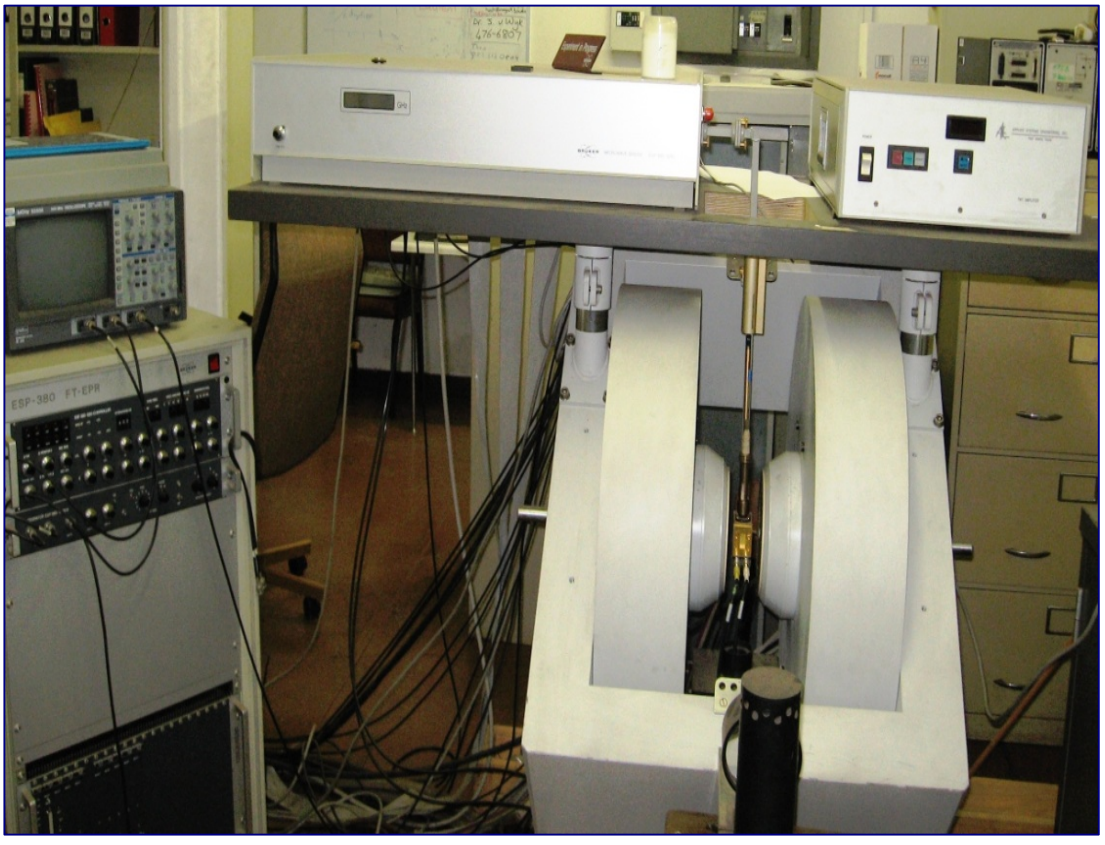

Figure 3.4: ESR spectrometer unit at the University of the Witwatersrand.

Shown in Fig. 3.5 is a classic ESR spectrum obtained from type 1b diamond. The integrated area (output curve integrated twice to give absorption curve area) of the absorption signal from the ESR spectrum represents the number of lone electrons, which in this case represents [N_s]. The concentration in a given diamond sample is determined by comparing the absorption curve area of that sample with a calibrated reference sample. Values of N_s levels for the examined diamond crystals are presented in Table 3.1. The much higher levels of N_s impurities of the HPHT sample compared to its CVD counterparts observed in this study could be related to the method usually used for the growth of diamond by the HPHT technique. As demonstrated in Table 3.1 the [N_s] of an OG CVD diamond crystal is always, at least a factor of two more than that of its DG counterpart. It is known that N is deliberately introduced during the growth of CVD OG diamonds (private communication).

3.5 Fourier transform infrared (FTIR) absorption spectroscopy

Infrared (IR) spectroscopy is the absorption measurement of IR frequencies by a sample placed in the path of the IR beam. It is a common spectroscopic technique for both qualitative and quantitative (with a suitable software algorithm) analyses. An IR spectrum represents a fingerprint of a sample with absorption peaks which correspond to the frequencies of vibrations between the bonds of the atoms making up the material in question.

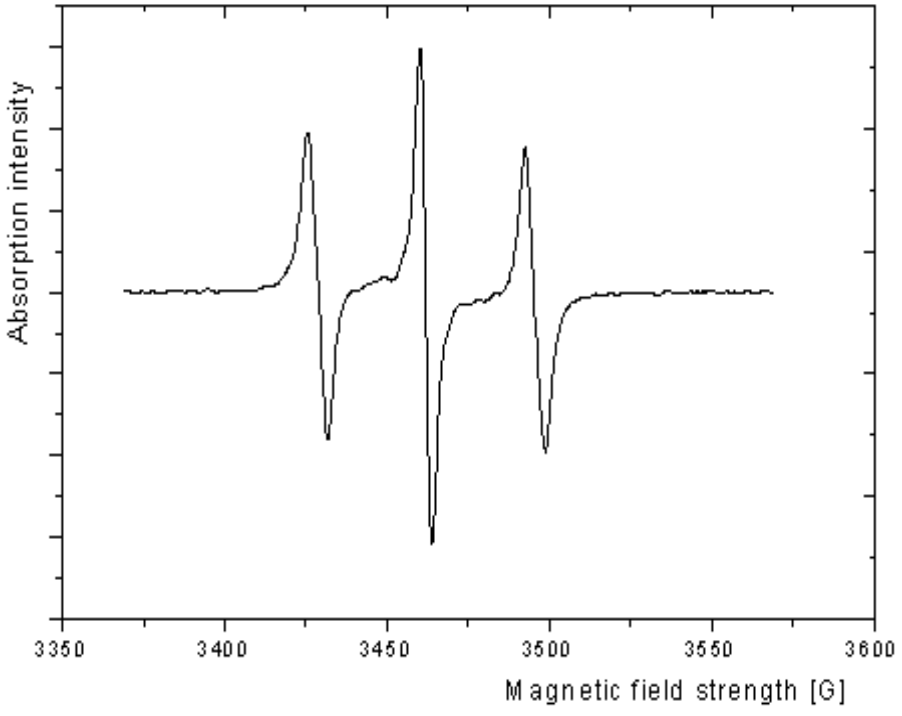

Figure 3.5: A classic ESR spectrum of single substitutional nitrogen in type 1b diamond.

At temperatures above absolute zero, atoms in molecules are in continuous vibrations relative to each other. The molecular vibrations (stretching and bending) are measured by the absorption of radiation of certain energies that corresponds to the vibration of excitation of the molecule from states $v = 0$ to $v = 1$. When the frequency of a particular vibration matches the frequency of the IR radiation focused on the molecule, the molecule absorbs the radiation. Every atom in a given molecule of a material has three degrees of freedom, which correspond to motions along any of three Cartesian coordinate axes (x, y, z) (Hsu, 1998). The dipole moments of the molecules change due to absorption of light of certain energies. The transition occurs by absorption of IR radiation if the transition integral is non-zero. The transition moment integrals are of the form:

$$\int \psi_v^0 x \psi_v^f d\tau \qquad \textbf{(3.1)}$$

$$\int \psi_v^0 y \psi_v^f d\tau \qquad \textbf{(3.2)}$$

$$\int \psi_v^0 z \psi_v^f d\tau \qquad \textbf{(3.3)}$$

where ψ_v^0 and ψ_v^f are the wave functions for the initial and final states, respectively involved in transitions. Dispersive IR spectrometers introduced in the mid-1940s are now replaced by FTIR spectrometers due to their superior speed and sensitivity (Hsu, 1998). Fourier Transforms are valuable tools for the spectral analysis of signals. A Fast Fourier Transform employs a fast algorithm for the computation of Discrete Fourier Transforms (Diman Batenkov, 2005). In FTIR spectrometers, all frequencies are examined simultaneously unlike dispersive spectrometers whereby each component frequency is examined in sequence. An IR absorption spectrum is usually a plot of absorption intensity or percent transmittance as a function of wavenumber (v) or wavelength (λ). The relationship between wavenumber and wavelength is of the form:

$$\boldsymbol{v\ (cm^{-1}) = \{1/\ \lambda\ (\mu m)\} * 10^4} \qquad \textbf{(3.4)}$$

Whereas ESR is a powerful tool for the characterisation of [N_s], IR spectroscopy provides a means for the identification of aggregate N in diamond and perhaps the estimation of their concentration (Kaminsky and Khachatryan, 2001). Whilst the vast majority of the N in natural diamond is found in aggregate forms where their free electrons tend to pair and no

paramagnetic resonance is observed, experimental evidence provided by McNamara (2003) suggested that aggregate N at least in the A form may exist in some CVD diamonds. In this study Mid-infrared absorption spectra were recorded using two different spectrometers from Bruker – a Tensor 27 IR spectrometer (Fig. 3.6(a)) at the University of the Witwatersrand and

(a)

(b)

Figure 3.6: The Vertex 70v (a) and Tensor 27 (b) IR spectrometers used for IR measurements

a Vertex 70v IR spectrometer at the University of Pretoria (Fig. 3.6(b)). Both spectrometers operate in the spectral range from 4000-400 cm^{-1}. A diamond ATR (attenuated total reflectance) cell as sample holder and the instrument chamber (Vertex 70v) were evacuated during spectra acquisition to eliminate interference from CO_2 and water vapour bands.

The FTIR absorption spectra recorded for the diamond crystals showed some distinct peaks within the spectral range from 1500 to 1050 cm^{-1} as illustrated in Fig. 3.7 for DGB1. However, only known peaks were identified and chosen for analysis. These included peaks occurring at 1090 (a feature characteristic of the A- and B-aggregates of N), 1282 (A-aggregate), 1430 (N3 nitrogen centre)[4] and 1481 (C-H centres) cm^{-1} (Zaitsev, 2001). A model for the N3 centre consists of three adjacent N atoms surrounding a vacancy whereas the C-H centres are deformational modes of sp^2-hybridised C-H bonds. Since peak areas are generally considered to be more reliable than both peak heights and FWHM as a measure of intensity which represents defect concentration, the integrated areas under the peaks were determined (Table 3.1). ORIGIN 8.0 software package was used for both baseline insertion and background subtraction. The data taken with the Tensor 27 and Vertex 70V spectrometers agreed to within 10%.

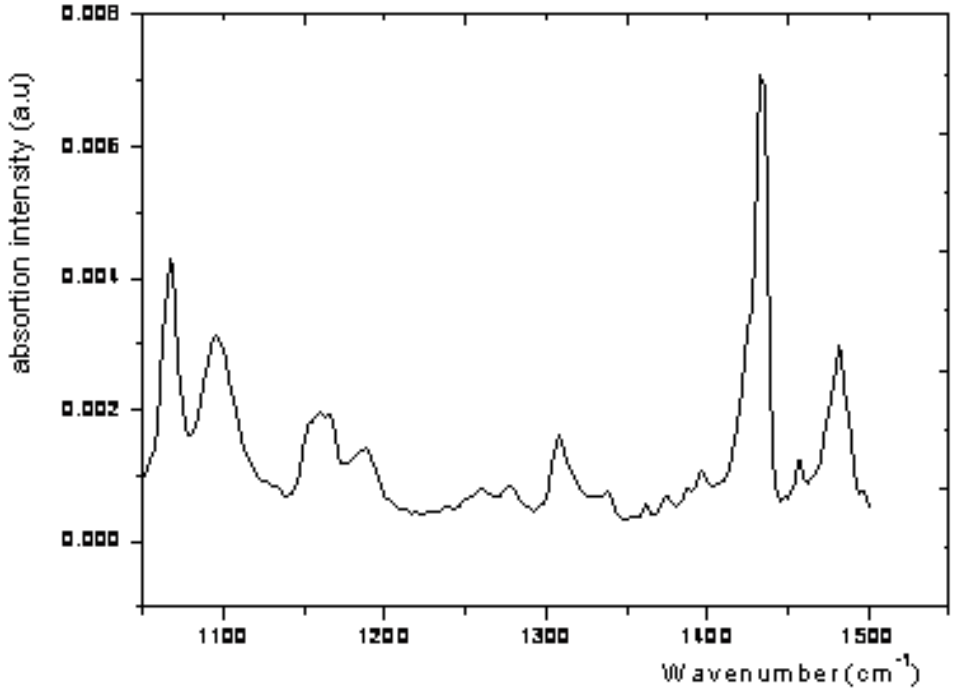

Figure 3.7: Fourier Transform infrared absorption spectrum of DGB1.

[4] There is a controversy surrounding the IR absorption at 1430 cm^{-1} as explained in chapter seven.

3.6 Thermoluminescence (TL) measurements

TL is a luminescence phenomenon of a material (an insulator or a semiconductor) which can be observed when the material is thermally stimulated (Bos, 2007). TL is different from the light spontaneously emitted from a substance when heated to incandescence in the sense that TL is the thermally stimulated emission of light following the previous absorption of energy from ionizing radiation at a sufficiently low temperature. A TL material is therefore a material that when first irradiated by ionizing radiation at or near room temperature, absorbs some energy which is stored. The stored energy is then released in the form of optical radiation (visible light) when the material is later heated in a readout device at a higher temperature.

When a TL material is exposed to ionizing radiation at a low temperature, a majority of the charge carriers become trapped at lattice imperfections. These carriers would remain trapped for a long period of time when stored at that or a lower temperature. When the temperature is raised by heating, the probability of escape is increased and the charge carriers are released from the traps, subsequently returning to a stable state with the emission of visible light. The optical radiation emitted by the TL material is related to the integrated radiation dose it has received during exposure to ionizing radiation. The storage capacity of a TL material (now known as a TL dosimeter or TLD) thus makes it suitable for dosimetric applications.

In this study, TL emission was used as a tool to scan the performances of the crystals since it gives an idea of the concentration of defects or trapping centres present within a given crystal. Two types of trapping levels are known: shallow levels, which are unstable at room or near room temperature and deep levels which remain stable at room temperature (Guerrero et al. 2004; Bergonzo et al., 2007). While the shallow traps are considered to be located at an energy level < 1.55 eV, deep trapping centres occur at energy levels > 2.2-0.1 eV (Assiamah, 2004). It is well-known that polycrystalline CVD diamonds have a large concentration of grain boundaries (Balducci et al., 2005) where electron traps are concentrated, or in more defective regions (Manfredotti et al., 2006). The presence of trapping centres reduces the lifetime of generated carriers in the conduction and valence bands. The density of trapping centres, N_T can be calculated from (Nebel, 2003):

$$N_T = 1/(\tau \upsilon_{th} \sigma_{cap}) \qquad (3.5)$$

where τ is the deep trapping carrier lifetime (≈340–550 ps), v_{th} is the thermal velocity of carriers (≈10^7 cm s^{-1}) and σ_{cap} is the capture cross section of traps (assumed to be equal to

10^{-15} cm^2 for neutral traps). Based on these parameters, Nebel (2003) obtained a value of 10^{17} cm^{-3} for the density of traps most likely to be present at grain boundaries in polycrystalline CVD diamonds.

The TL measurements were carried out under subdued light conditions (to minimize light influences on TL response) by placing each irradiated diamond crystal (using a ^{90}Sr beta source with a controlled exposure time of 30 s and delay time before readout of 15 s) into a TLD reader - model Toledo 654 (Fig. 3.8). The temperature was ramped up to about 350^{o} C for luminescence-emission measurements. The TL response (define as TL emission per unit volume) values of the investigated crystals are displayed in Table 3.1. A higher TL response implies a more defective crystal which could reflect the greater presence of trapping levels.

3.7 Production of electrical contacts on diamond surfaces

Electrical contacts were deposited on opposite surfaces of each crystal by thermal evaporation of successive angstrom thick layers of Ti (200 Å)/Pt (200 Å)/Au (2000 Å) in similar procedures as reported by Assiamah (2004) and Mavunda (2008). Titanium (Ti) was deposited first as its forms a strong carbide layer with diamond interface. This was followed by platinum (Pt) and then gold (Au) which protects the contact by preventing oxidation due to its chemical inertness. While the contacts almost cover the entire surface of the two

Figure 3.8: Thermoluminescence unit showing the TLD reader (model Toledo 654)

opposite faces of each diamond, extra precautions were taken to ensure that the peripheral edges are not contaminated by any of the metallic layers to avoid short-circuiting between the contacts. Finally, the metallized crystals were annealed in a ceramic vacuum furnace at a temperature of 500 ^{o}C and pressure of 10^{-6} torr.

3.8 Presentation of prototype design of multi-purpose synthetic diamond probe

It was pointed out in chapters one and two that the overall performance of an ionizing radiation detector depends largely on its design. A good design should be such that it limits parameters that have a negative influence on dosimetric accuracy such as perturbation and energy dependent effects represented by the term $\left\{\left(\frac{\overline{L}}{\rho}\right)_{\det}^{med}.P_{pert}\right\}$ as depicted in Eq. (1.3) (chapter one). Realising that a tissue-equivalent detector can reduce such influencing quantities, extra care has to be exercised in the design and construction of the detector with emphasis on its encapsulation and contact material as it is known that high atomic number materials used to form ohmic contacts can introduce an element of energy dependence (Laub et al. 1999; Górka et al., 2008). Furthermore, as high impedance devices and materials such are diamonds are susceptible to the presence of noise, deliberate precautions have to be adopted to exclude all ambient interferences on the sensing element and associated equipment so as to exploit the full potential of diamond as a sensor for ionizing radiation. Additionally, the orientation of the detector material and its holder should be such that rotational uncertainty is eliminated.

Considering the implication of Eq. (1.3) in clinical dosimetry including factors that influence dosimetric accuracy, the limitations and major challenges of commercial radiation detectors one of which is to achieve high radiation sensitivity or SNR for measurements in small fields, it is therefore the objective of this study to present:

- a radiation probe that is constructed of entirely (for the part placed in radiation fields of sizes up to 20 x 20 cm^2) near-tissue equivalent material;

- a probe that is homogenous in design and construction with minimal energy dependence perturbation effects and with very low leakage current or stable background signal;
- a probe that is easy to manufacture and assemble, and which is compatible with commercially available electrometer systems;
- a probe that is invulnerable to environmental influencing factors such as electromagnetic disturbances;
- a probe that is practical and simple to use, and that ensures ease of positioning the sensor face to the impinging radiation field for accurate dose measurements;
- a probe with minimal angular dependence and cable effects;
- a probe that will not require daily pre-irradiation;
- a multi-purpose and cost effective probe that is suitable for dose measurements of both low-energy X-rays and high-energy radiotherapy beams in large as well as in small radiation fields.

Illustrated in Fig. 3.9 is a 3D configuration of the synthetic diamond probe. It is constructed using tissue-equivalent materials with four carbon-fibre rods (electrodes) providing electrical contacts and shielding. Design aspects of the probe have been patented by (Nam and Ade, 2011 - 2013).

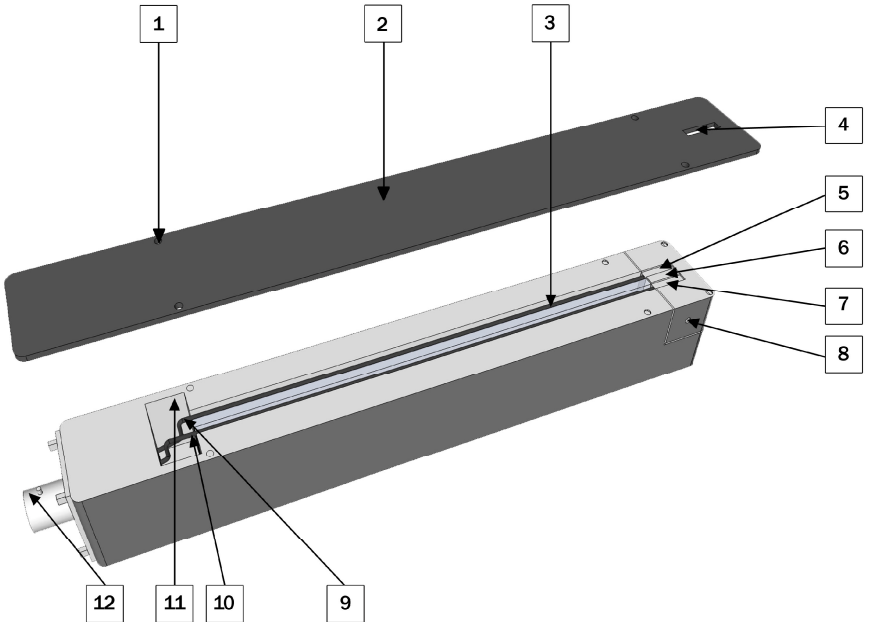

Figure 3.9: 3D configuration of the synthetic diamond probe

The diamond crystal (6), with ohmic contacts deposited on its two opposite faces is sandwiched between two thin tissue-equivalent insulating boards (5 and 7) each of size 10 x 10 mm^2 and each with conductive surfaces on opposite faces. Examples of such insulating board materials which could be used are Teflon and Mylar or "Solid Water" RMI 57 boards manufactured by Gammex with carbon/graphite coating on opposite faces. Conductive adhesive provided electrical connections between the four electrodes and the surfaces of the insulating boards (5 and 7). To ensure proper electrical contact between the diamond sensor (6) with pre-metalized surfaces and boards (5) and (7), pressure is provided via a Teflon based screw (8).

The four electrodes are located within two channels, with each channel housing a pair. Rib (3) provides a means to separate the two channels. Of the pair of electrodes, one electrode makes electrical contact to one surface of the boards (5 and 7) and the other to the opposite surface. To reduce electromagnetic disturbance, each of the two electrodes that are used to provide electrical contacts from the diamond surfaces is fed through an insulating tube which in turn is covered with a conductive sleeve-tubing.

Electrical connections to external electronics are carried out through the use of a standard tri-axial connector (12). Gold plated conductive clips with insulated wires (9 and 10) attached are used to connect onto the rods. The space in recess (11) in the probe body provides the necessary access for such connections to be made. The other ends of the wires are soldered directly onto the tri-axial connector. Since commonly available electrometers are typically three terminal systems, the input to the electrometer is provided by a tri-axial cable with the sensor connected to the other end. The central conductor is connected to the high input impedance of the electrometer whilst the intermediate conductor is connected to the low impedance input. The outer braid of the cable is connected to ground. A schematic cross-section of the probe illustrating the electrical connections is presented in chapter 4.

Unlike the typical designs of diamond detectors often encountered in literature (Heydarian et al., 1993; van der Merwe et al., 1999; Manfredotti et al., 1998; Marczewska et al., 2007; Assiamah et al., 2007; Lansley et al., 2009; Betzel et al., 2010; Tromson et al., 2010; Schirru et al., 2010; De Angelis et al., 2010) where the diamond plate is fixed in a cylindrical housing, in this thesis the sensor plate is encapsulated in a holder that is rectangular in shape and constructed of tissue-equivalent Perspex body. The detector housing can hold plates of

diamond crystals of various sizes and types. Crystals of sizes as large as 10 x 10 mm^2 can be accommodated. Its construction and configuration is such that it allows for radiation detection in both 'edge-on' and 'flat-on' exposure orientations[5] (Fig. 3.10) without having first to re-orient the diamond within the body of the probe. As such the probe is suitable for accurate determination of absorbed radiation dose from low-energy X-rays such as those emitted by mammography X-ray units and also absorbed dose from high-energy radiotherapy beams. The configuration further allows features such as shielding against interferences from ambient light and electromagnetic interferences to be easily incorporated and as well allows associated equipment such as phantoms to be cost effectively manufactured.

The entire body of the probe is made up of Perspex. A Perspex probe-cover (2) has a thin window (4) which could be used for the direct measurement of incident radiation, that is, at zero depth. To minimise the interferences from ambient light, the body of the probe is covered with a thin opaque coating. This, in turn, obviates the need to pre-irradiate the detector prior to dose measurements. The results of the study are presented in chapter five.

For the presented diamond probe, the intermediate (or inner) conductor is utilized to divert unwanted signals (see chapter 4 for circuit diagram). Each of the two main carbon-fibre electrodes that are used to collect the charge carriers created within the diamond sensor, has a conductive sleeve around the insulating tube through which the electrode passes.

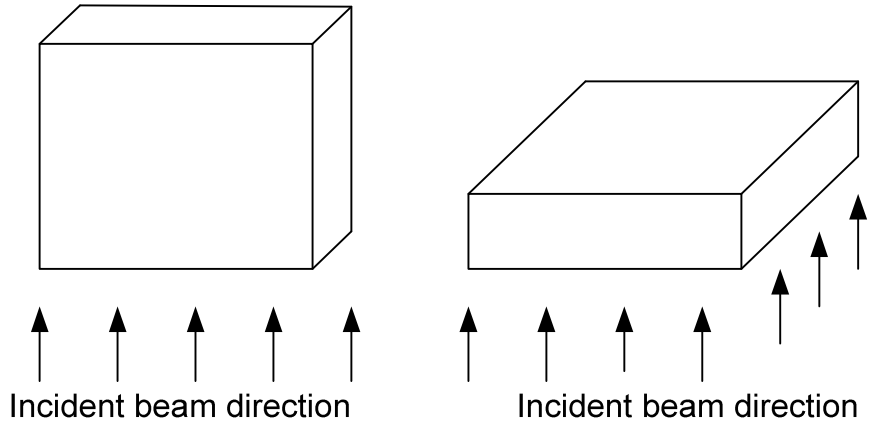

Figure 3.10: The "Edge-on" (Left) and "Flat-on" (Right) exposure configurations of the probe

[5] In the 'edge-on' orientation, the incident radiation is normal to the edge of a diamond wafer hence a smaller surface area but greater attenuation depth. In the 'flat-on' orientation, the incident radiation is normal to the face of the diamond, consequently a larger area but reduced attenuation depth.

The conductive sleeves are in turn connected to the low impedance input. This serves to suppress interferences. To further minimize interferences, the two insulating boards, with the diamond sensor sandwiched in between as described above, are provided. The outer carbon-fibre electrodes that are connected to the outer surfaces are in turn connected to the inner conductive layer of the tri-axial cable. Each of the boards (with the carbon fibre rods electrically connected to each face) thus serves two functions: one of which is to collect the charge carriers created within the diamond sensor and the other is to shield the diamond sensor against surrounding interferences. The latter is done by diverting any unwanted signals created to the low impedance input of the electrometer.

Figure 3.11 shows the design of a customised solid Perspex phantom (with the probe inserted) which could be used for performing absorbed dose and other dosimetric measurements. The figure highlights the manner in which the probe fits squarely into the phantom. The purpose of the phantom is to simulate the radiation absorption properties of the human body. To obtain the depth dose profile measurements of the impinging radiation beam after it has passed through tissues of varying thicknesses, uniform sheets of Perspex of varying thickness are stacked on top of the probe-in-phantom unit. If there is need for the probe to be used in a water phantom instead of a plastic phantom, the body of the probe could easily be made water-proof. Furthermore, for free in-air, directional dependence measurements, the probe can be fitted with a circular Perspex build-up cap. Shown in Fig. 3.12 is an image of such a cap.

Providing a circular opening directly opposite to the locating screw 8 (Fig. 3.9) on the removable piece of the main Perspex housing and replacing solid board (7) with a board having a hole that is covered with a thin film, allows the probe to be used both for zero depth measurements under “flat-on” conditions and for charged particles measurements.

3.9 Electrical characterization

Before conducting dosimetric measurements, the electrical quality of the synthetic diamond detectors were evaluated by investigating and measuring the leakage current of each crystal, as it is known that background signals and their fluctuations are an unwanted noise source in radiation measurements and can limit the magnitude of the applied electric field (Kania, 1993). In addition, the sensitivity of a diamond detector depends on the SNR (Manfredotti et al., 1998). Dark current or reverse bias leakage current, as it is referred to in non-optical

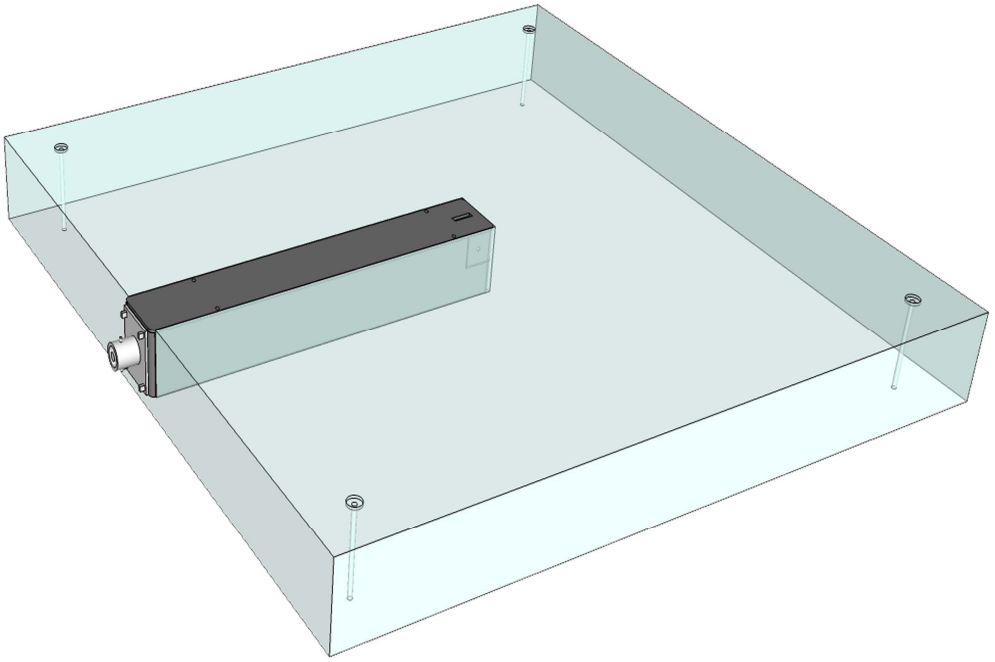

Figure 3.11: 3D configuration of the probe-in-phantom unit demonstrating the manner in which the probe fits into the solid phantom. Rotational uncertainty is eliminated in such configuration.

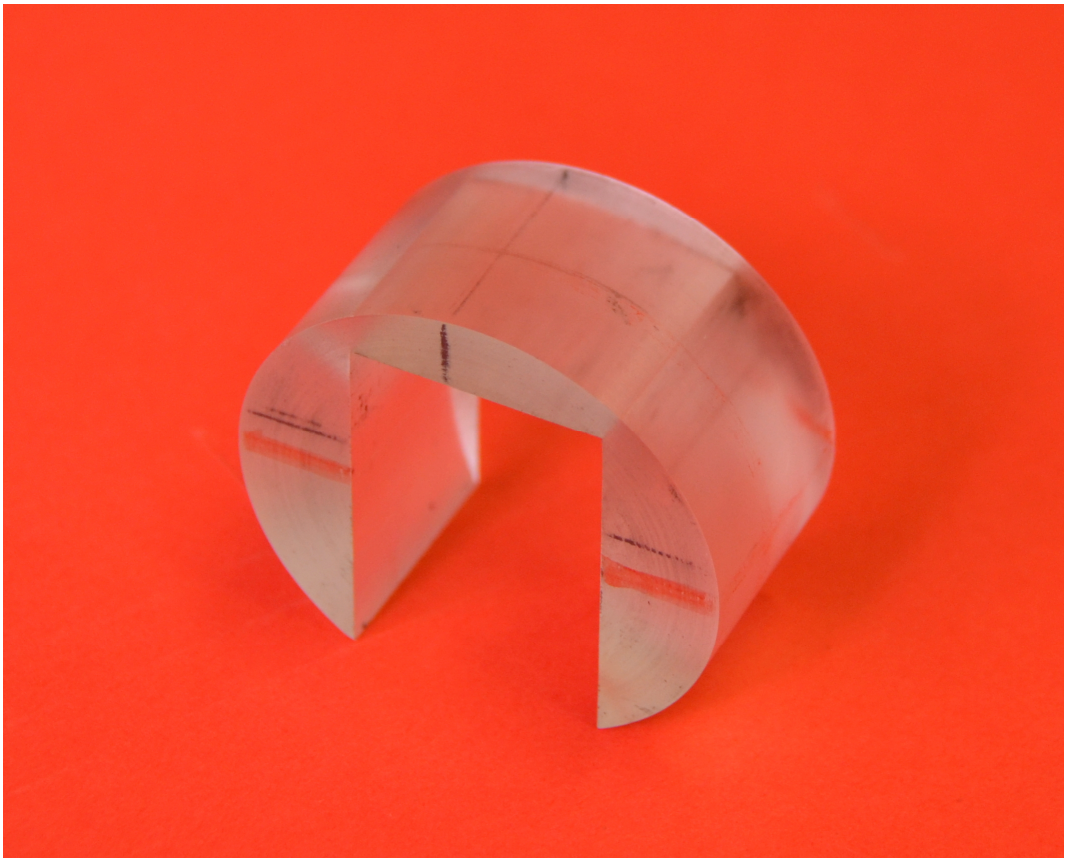

Figure 3.12: Image of circular build-up cap for free in-air angular dependence measurements

systems, is the relatively small electric current that flows through a device in the absence of irradiation, and its magnitude could be influenced by a number of factors including contact material.

In this study the leakage current of each diamond detector was observed to be greatly influenced by ambient light when the diamond probe was connected to a PTW Unidos E electrometer system. The leakage current was also found to increase with applied voltage (see chapter 4). When the diamond probe was shielded from ambient light and connected to Unidos E electrometer with a connecting cable of about 10 m in length in a clinical environment, the diamond detectors showed initial dark current values in the range from ~ 0.01 to 0.35 nA at 1.0 kV/cm under dark conditions (in the absence of irradiation) with the HPHT sample showing the smallest value and DGA1 showing the highest value. After radiating the crystals with high-energy radiation, the current of each diamond sensor increased and then dropped within a few seconds to their initial values with that of the HPHT crystal decaying faster than its CVD counterparts. The reason for this observation could be ascribed to the influence of defect levels as high leakage currents in CVD diamonds have been attributed to graphitic contaminations at grain boundaries (Górka, 2008).

The results presented in Table 3.1 indicate that the CVD diamond crystals are more defective compared to the HPHT diamond. Displayed in Table 3.1 are dark current density (J_o) values of the diamond crystals at 1.0 kV/cm (i.e., at 50 or 100 V bias for 0.5 or 1.0 cm thick crystals, respectively). The J_o values (computed as dark current per surface area of contact) for the composite contacts that comprise an angstrom thickness for the three layers of Ti/Pt/Au metals compare favourably with or better than the values of 6.3×10^{-9}, 4.1×10^{-8} and 1.5×10^{-5} at 20 V bias reported in literature for Pt, Al, and Au contacts, respectively (Dismukes et al., 1993). Table 3.1 thus indicates i.t.o electrical quality that the HPHT diamond and DGB1 show an overall better performance.

3.10 Dosimetric equipment and measurement techniques

All dosimetric measurements taken with the prototype synthetic diamond probe were from exposures to mammography X-rays in the energy range from 25-32 kVp produced by a Senographe 500T mammography X-ray machine, a ^{60}Co teletherapy machine (Thetratron Equinox) and a Siemens Primus linear accelerator (linac) (Fig. 3.13) at the Charlotte Maxeke Johannesburg Academic Hospital. The linac has the capability of providing both high-energy

electron (5 -14 MeV) and X-ray photon (6 and 15 MV) beams. As the probe is being evaluated for dosimetric applications, similar irradiation geometries and parameters typically used clinically were utilised. Detectors commonly used for the dosimetry of high-energy electron and photon beams were employed for comparative measurements. These include a 0.055 cc Markus chamber (Type 23343), a 0.66 cc Farmer-type chamber and a small-field diode detector (Diode E).

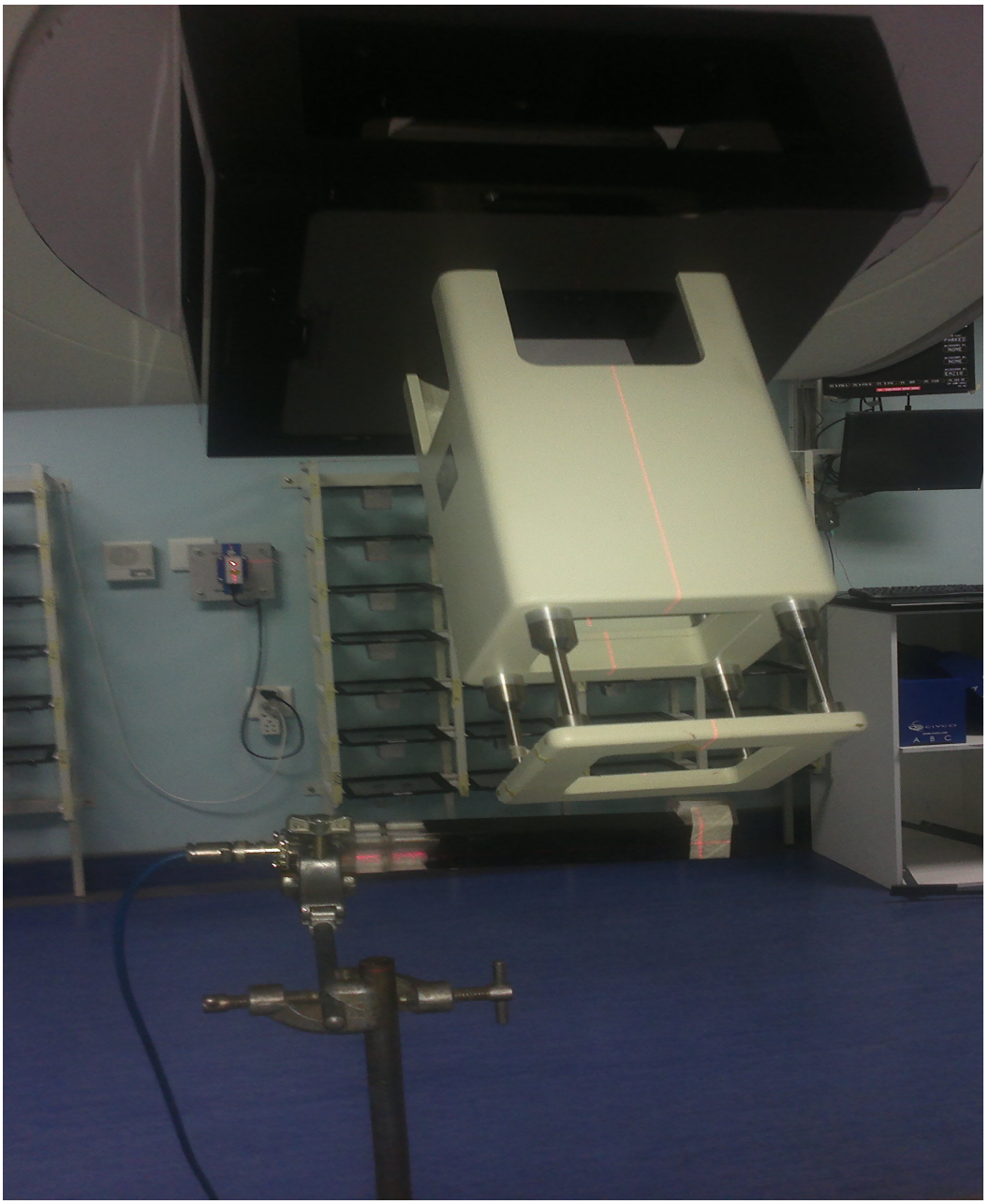

Figure 3.13: Experimental setup for free in-air angular dependence measurements under exposure to an electron beam delivered by a linac.

Given that the presented prototype probe is still in the research phase and has not been calibrated for absolute dosimetry, and given the importance of relative dosimetry in radiotherapy, relative beam data such as electron percent depth-dose (*PDD*) data, ^{60}Co tissue-maximum ratios (*TMR*s) and output factors (*OF*s) for both electron and photon beams are basically used as tools in this thesis to characterise the performance of the diamond probe. These three vital beam parameters (defined in subsequent chapters and Appendix A) show the variation of the relative dose plotted either as a function of depth (*PDD* and *TMR*) or field size (*OF*) and are used to establish treatment charts or curves. Since these parameters could be largely influenced by noisy background, energy and/or dose rate dependence, any significant deviation between the performances of the diamond probe and a reference detector such as an ion chamber would indicate their presence and therefore it is crucial to select a crystal material and/or design a radiation probe whose overall performance is independent of such influencing quantities.

Other dosimetric measurements include: angular and dose rate dependence measurements; measuring the response of the diamond probe with varying applied voltage for bias voltage selection; linearity of the probe's response with absorbed dose for electron beams, exposure parameters (tube loading and nominal tube voltage) for mammography X-rays and timer for ^{60}Co photons. Also, the SNR and radiation sensitivity of the diamond probe were determined and a systematic study of the instability of response of the diamond sensors requiring pre-irradiation was conducted. Because of the influential role of the dose rate linearity index Δ in dosimetry, a greater part of the project is focused on a study of the dose rate dependence of the synthetic diamond detectors.

3.11 Initial dosimetric evaluation of the performance of the presented probe

In order to determine whether the probe has been optimized (i.t.o various influencing quantities such as environmental and positional factors, encapsulation and contact materials) for the evaluation of the performances of the diamond detectors under clinical conditions, initial dosimetric characterizations were conducted on exposure to low-energy X-rays and megavoltage electrons (chapter 4) having coupled a detecting element (HPHT1, labelled simply as HPHT) selected from the characterized samples. The HPHT sample was chosen for this part of the study because of its very low and stable leakage current.

Following the results of the initial study, further dosimetric characterizations on exposure to low-energy X-rays and high-energy electrons and photons were then undertaken on the various diamond detectors so as to evaluate the influence of defect levels on detector performances within an optimized probe, the results of which are reported in subsequent chapters. The relationship between detector size and field size under small-field conditions was also investigated utilizing the various diamond crystals as sensing elements.

Whereas the results of various dosimetric characterizations using low-energy X-rays and high-energy electron and photon beams are presented in chapters 4 to 8, those employing ^{60}Co radiation are presented in Appendix A.

References

Ascarelli, P., Cappelli, E., Trucchi, D.M., Conte, G., 2003. CVD diamond dosimetric response evaluated by X-ray absorbers method. *Diamond Relat. Mater.* **12**, 691.

Assiamah, M., 2004. Dosimetric techniques for mammography mass screening programs. *PhD Thesis, University of the Witwatersrand, Johannesburg***.**

Assiamah, M., Nam, T.L., Keddy, R.J., 2007. A synthetic diamond probe for low-energy X-ray dose measurements. *Appl. Radiat. Isot.* **65**, 545.

Balducci, A., Macro Marinelli, Milani, E., Morgada, M.E., Prestopino, G., Scoccia, M., Tucciarone, A., Verona-Rinati, G., 2005. Trapping-detrapping defects in single crystal diamond films grown by chemical vapor deposition. *Appl. Phys. Lett.* **87**, 222101.

Balmer, R.S., Brandon, J.R., Clewes, S.L., Dhillon, H.K., Dodson, J.M., Friel, I., Inglis, P.N., Madgwick, T.D., Markham, M.L., Mollart, T.P., Perkins, N., Scarsbrrok, G.A., Twitchen, D.J., Whitehead, A.J., Wilman, J.J, Woollard, S.M., 2009. Chemical vapour deposition synthetic diamond: materials, technology and applications *J. Phys.: condens. Matter* **21**, 364221.

Bergman, L., Nemanich, R.J., 1995. Raman and photoluminescence analysis of stress state and impurity distribution in diamond thin films. *J. Appl. Phys.*, **78**, 6709.

Bergonzo, P., Tromson, D., Descamps, C., Hamrita, H., Mer, C., Tranchant, N., Nesladek, M., 2007. Improving diamond detectors: A device case *Diamond Relat. Mater.* **16**, 1038.

Betzel, G.T., Lansley, S.P., Baluti, F., Reinisch, L., Meyer, J. 2010. Operating parameters of CVD diamond detectors for radiation dosimetry. *Nucl. Instrum. Methods Phys. Res*. A **614**, 130.

Blum, F., Denisenko, Job, A.R., Borchert, D., Weber, W., Borany, J.v., Hilleringmann, U., Fahrne, W.R., 1998. Nuclear Radiation Detectors on Various Type Diamonds. *IEEE*, 2382.

Boss, A.J.J., 2007. Theory of thermoluminescence. *Radiation Measurements* **41**, S45.

Catledge, S.A, Vohra,Y.K., Ladi, R., Rai, G., 1996. Micro-Raman stress investigations and X-ray diffraction analysis of polycrystalline diamond (PCD) tools. *Diamond Relat. Mater.* **5**, 1159.

De Angelis, C., Bucciolini, M., Viscomi, D., Marczewska, B., Onori, S., 2010. Characterization of a HPHT diamond detector for clinical applications. *Nucl. Instrum. Methods Phys. Res*. A **612**, 576

Dima Batenkov, “Fast Fourier Transform”. Key papers in Computer Science, Seminar 2005.

Dismukes, J. P., Ravi, K.V., 1993. Proceedings of the 3rd International Symposium on Diamond Materials – *Nature*.

Erasmus, R.M., Comins, J.D., Mofokeng, V., Martin, Z., 2011. Application of Raman spectroscopy to determine stress in polycrystalline diamond tools as a function of tool geometry and temperature. *Diamond Relat. Mater*. **20**, 907.

Faggio, G., Marinelli, M., Messina, G., Milani, E., Paoletti, A., Santangelo, S., Verona-Rinati, G.,1999. Structural characterisation of ionising-radiation detectors based on CVD diamond films. *Microsystem Technologies*, **6**, 23.

Fallon, P.J., 1989. Synthetic diamonds as pulse counting radiation detectors. MSc Dissertation University of the Witwatersrand, Johannesburg.

Fish, M.L., Massler, O., Reid, J.A., MacGregor, R., Comins, J.D., 1999. The application of photoluminescence and Raman spectroscopy of synthetic diamond. *Diamond Relat. Mater.* **8**,1511.

Fowler, J.F., 1966. Solid state electrical conductivity dosimeters. Radiation Dosimetry. vol. II. New York: Academic. pp 291.

Górka, B., Nilsson, B., Svensson, R., Brahme, A., Ascarelli, P., Trucchi, D.M., Conte, G., Guerrero, M.J., Tromson, D., Rebisz, M., Mer, C., Bazin, B., Bergonzo, P., 2004. Requirements for synthetic diamond devices for radiotherapy dosimetry applications *Diamond Relat. Mater.* **13**, 2046.

Górka, B., 2004. Development of tissue-equivalent CVD-diamond radiation detectors with small interface effects. PhD Thesis, Stockholm University.

Heydarian, M., Hoban, P.W., Beckham, W.A., Borchardt, I.M, Beddoe, A.B., 1993. Evaluation of a PTW diamond detector for electron beam measurements. *Phys. Med. Biol*. **38**, 1035.

Hoban, P.W., Heydarian, M., Beckham, W.A., Beddoe, A.H., 1994. Dose rate dependence of a PTW diamond detector in the dosimetry of a 6 MV photon beam. *Phys. Med. Biol*. **39**, 1219.

Hsu, C.P.S, Infrared spectroscopy, in: F.A. settle (Ed.), Handbook of Instrumental Techniques

for Analytical Chemistry, Prentice-Hall, Inc, New Jersey, 1998, pp 247-283.

Kalish, R., 2008. Design and characterization of a tissue-equivalent CVD-diamond detector for clinical dosimetry in high-energy photon beams. *Physica Medica,* **24**, 159.

Kaminsky, F.V., Khachatryan, G.K., 2001. Characteristics of nitrogen and other impurities in diamond as revealed by infrared absorption data. *The Canadian Mineralogist,* **39**, 1733.

Kania, D.R., Landstrass, M.I., Plano, M.A., 1993. Diamond radiation detectors. *Diamond Relat. Mater.* **2**, 1012.

Kirillov, D., Reynolds, G.J., 1994. Linewidths of phonon lines of natural and synthetic diamonds. *Appl. Phys. Lett.* **65**, 1641.

Knight, D.S., White, W.B., 1989. Characterization of diamond films by Raman spectroscopy. J. Mater. Res. **4**, 385.

Lansley, S.P., Betzel, G.T., Meyer, J., Baluti, F., Reinisch, L., Meyer, J., 2009. Investigation of the suitability of commercially available CVD diamond for megavoltage X-raydosimetry. *Nucl. Instrum. Methods Phys. Res.* A **607**, 659.

Laub, W.U., Kaulich, T.W., Nusslin, F., 1999. A diamond detector in the dosimetry of high-energy electron and photon beams . *Phys. Med. Biol.* **44**, 2183.

Loubser, J.H. N., van Wyk, J.A. *Diamond Conference*, Reading, UK, 1981 (unpublished).

Manfredotti, C., Apostolo, G., Fizzotti, F., Lo Giudice, A., Morando, M., Pignolo, R., Polesselo, P., Truccato, M., Vittone, E., Nastasi, U., 1998. CVD diamond tips as X-ray detectors. *Diamond Relat. Mater.* **7**, 523.

Manfredotti, C., Vittonea,E., Paolini, C., Olivero, P., Lo Giudice, A., 2006. Blue light sensitization of CVD diamond detectors. *Diamond Relat. Mater.* **12**, 662.

Marczewska, B., Kupriyanov, I., Pal'Yanov, Yu., Nowak, T., Olko, P., Rębisz, M., Waligórski,

M.P.R., 2007. A study of radiation dosimeters based on synthetic HPHT diamond. *Diamond Relat. Mater.* **16**, 191.

Mavunda, R.D., Zakari, Y.I., Nam, T.L., Keddy, R.J., 2008. The presence of defects and their influence on the performance of CVD diamond as an α-particle radiation sensing element. *Appl. Radiat. Isot.* **66,** 1128.

Mavunda, R.D., 2008. Evaluation of radiation detector systems for mammography X-ray units.

PhD Thesis, University of the Witwatersrand, Johannesburg.

McNamara, K.M., 2003. Aggregate nitrogen in synthetic diamond. *Appl. Phys. Lett.* **83**,

1325.

Nam, T.L., Ade, N. 2011. Improved Multi-purpose Ionizing Radiation Detector. SA Patent 2011/07889.

Nam, T.L., Ade, N. “Radiation Probe”, Functional Design Applications: SA Patent registered (F2012/02184); EU registered (002 239 889-001); China accepted (2013 302 225 167); Japan accepted (2013-012009); US pending (FD29/456,332).

Nam, T.L., Karfunkel, U., Keddy, R.J., Every, A.G., 1991. The effect of nitrogen impurity on the radiation detection properties of synthetic diamond. Radiat. Eff. Def. Solids **116**, 233.

Nam, T.L., 1989. Nuclear radiation detection properties of diamond. *PhD Thesis, University of the Witwatersrand, Johannesburg*.

Nebel, C.E., Waltenspiel, A., Stutzmann, M., Paul, M., L. Schäfer, L., 2000. Persistent photocurrents in CVD diamond. *Diamond Relat. Mater.* **9**, 404.

Pickard, C.D.O., Davis, T.J., Wang, W.N., Steeds, J.W., 1998. Mapping crystalline quality in diamond films by micro-Raman spectroscopy. *Diamond Relat. Mater.* **7**, 238.

Prawer, S., Nemanich, R., 2004. Raman spectroscopy of diamond and doped diamond. *Phil. Trans. R. Soc. Lond.* A **362**, 2537.

Schirru, F., Kisielewicz, K., Nowak, T., Marczewska, B., 2010. Single Crystal Diamond Detector for Radiotherapy. *J. Phys. D: Appl. Phys.* **43**, 265101.

Tranchant, N., Tromson, D., Descamps, C., Isambert, A., Hamrita, H., Bergonzo, P., Nesladek,

M., 2008. High mobility single crystal diamond detectors for dosimetry: Application to radiotherapy. *Diamond Relat. Mater.* **17**, 1297.

Tromson, D., Rebisz-Pomorska, M., Tranchant, N., Isambert, A., Moignau, F., Moussier, A., Marczewska, B., Bergonzo, P., 2010. Single crystal CVD diamond detector for high resolution dose measurement for IMRT and novel radiation therapy needs. *Diamond Relat. Mater.* **19**, 1012.

Van der Merwe, D.G., Keddy, R.J., 1999. Relative electron dosimetry using a synthetic diamond probe. *Radiat. Phys. Chem.* **54**, 325.

Walker, J., 1979. Optical absorption and luminescence in diamond. *Rep. Prog. Phys.* **42**, 16o6.

Zaitsev, A.M. Optical Properties of Diamond, Springer Edition, 2001.